Norwegian University
of Life Sciences

Master's Thesis 2020 60 ECTS
Faculty of Environmental Sciences and Natural Resource Management

The toxicity of depleted uranium and uranium nanoparticles in the nematode *Caenorhabditis elegans*

Aleksander Sverdrup Aarsand
Chemistry and Biotechnology

Preface

This thesis is the final part of an integrated masters program in chemistry & biotechnology at the Norwegian University of Life Sciences (NMBU). The project was funded by Centre for Environmental Radioactivity (CERAD) and all experimental work was performed in the Isotope lab at NMBU. The work was supervised by Dr. Dag Anders Brede (main-supervisor) and Dr. Lisa Magdalena Rossbach (co-supervisor).

First, I would like to thank Dag for all his training and encouragement. His enthusiasm for both my work and the subject in general has been an inspiration. Thank you to Lisa for taking time to help me in the lab, and giving me feedback. Also, a sincere thanks to you both for reading my countless drafts, and for helping me improve my academic writing. I want to thank Karl Andreas Jensen for helping me with ICP-MS measurements, Ian Thomas Behnke Byrnes for helping me with nanoparticle preparation and characterization, and Erica Maremonti for helping me with fluorescence imaging. Thank you to everyone else at the Isotope lab for making me feel welcome.

Thank you to Kristine, Christopher and Lars Johan for making my time at Ås so enjoyable. Thank you to all the lovely and talented musicians in Studentstorbandet ved NMBU St. 1912. I am going to miss playing with you. A special thanks to my grandparents, Gunnar and Ragnhild, for helping me through the difficult times these last three years.

Aleksander Sverdrup Aarsand

Ås, December 2020

Abstract

In recent years, nanoparticles have been the subject of intensive research and have been shown to have unique toxic properties compared to bulk material. Nevertheless their toxic mechanisms, and thus their ecotoxicological risk potential are not well understood. Uranium nanoparticles are released into the environment from military activity, nuclear industry and during accidents, making the study if the fate and toxicity of U in the environment essential. Therefore, in the present work the toxicity of uranium UO_2 nanoparticles (NPs) and uranyl (UO_2^{2+}) ions was investigated using the nematode *Caenorhabditis elegans* as a model organism.

The UO_2 NPs were characterized in respect to size and surface charge. Dynamic light scattering (DLS) revealed a NP size of 174 ± 8.2 nm with a polydispersity index (PDI)of 0.25 ± 0.033. The zeta potential of the UO_2 NPs in de-oxygenated double distilled water (ddH_2O) water was -9.9 mV, indicating a low suspension stability. Transmission electron microscopy (TEM) micrographs revealed large NP agglomerates in the suspension, and a subsequent image analysis showed a NP size of 5 ± 1.4 nm.

In 96 hour exposure studies in moderately hard reconstituted water (MHRW) at pH 7.1-7.4, 100% mortality was observed at 277 µM UO_2^{2+} and 1100 µM UO_2 NP. In the UO_2^{2+} exposure study, a significant decrease in reproduction and growth was observed at 62 µM and higher, while no change in fertility was observed. In the UO_2 NP exposure there was a significant reduction in growth at 140 µM and higher, with a significant reduction in reproduction at 240 µM and higher. At 460 µM fertility was reduced to 0%. Nematodes exposed to 240 µM UO_2 in the form of NPs also displayed a disproportionately large pharynx, and swollen and malformed intestines. Regression analysis of exposure concentration and effect on reproduction showed that the dose-response from UO_2^{2+} was twice as high as for UO_2 NPs. Furthermore, 10% effect concentration (EC_{10}) and half maximum effect concentration (EC_{50}) values was calculated for reproduction in nematodes exposed to both UO_2^{2+} and UO_2 NPs, and were several times greater for the NPs than the ions. Thus, it was concluded that UO_2^{2+} is more toxic to the nematodes than UO_2 NPs

Total uptake and retained U after depuration was assessed in nematodes exposed to UO_2^{2+} and UO_2 NPs. Inductively coupled plasma mass spectrometry (ICP-MS) measurement revealed a higher uptake and retention in nematodes exposed to UO_2 NPs than UO_2^{2+}. This implies that even if the UO_2 NPs had a lower specific toxicity, this could lead to bioamplification in the environment.

Reactive oxygen specie (ROS) production was investigated as a possible toxic MOA using reporter strains of *C. elegans* and fluorescence microscopy. In the SOD-1 reporter strain there was a slight upregulation of the *sod-1* gene, which was only significant in nematodes exposed to UO_2 NPs. However, analysis of the HyPer and GRX biosensor strains produced no valid results, and this topic should be investigated further in future studies.

Samandrag

I dei siste åra har mykje forsking blitt gjort på nanopartiklar og dei har vist seg å ha unike toksiske eigenskapar samanlikna med tilsvarande bulkmateriale. Likevel er dei toksiske mekanismane, og dermed det økotoksiske risikopotensiale deira ikkje godt forstått. Uran (U) nanopartiklar (NP) blir sloppe ut i miljøet frå militær aktivitet, atomindustri, og under ulykker, noko som gjer det til ei essensiell oppgåve å undersøke skjebnen og toksisiteten til U i miljøet. Derfor vart i dette arbeidet, toksisiteten til UO_2 NP og uranylioner (UO_2^{2+}) undersøkt ved bruk av nematoden *C. elegans* som modellorganisme.

UO_2 NP vart karakterisert med omsyn på størrelse og overflateladning. Dynamisk lysspreiing (DLS) gav ein NP-størrelse på 174 ± 8,2 nm med ein polydispersitetsindeks (PDI) på 0,25 ± 0,033. Zeta potensialet til UO_2 NP i de-oksygenert dobbeldestillert vatn (ddH_2O) var -9,9 mV, ein indikasjon på låg stabilitet i suspensjonen. Transmisjonselektronmikroskopi (TEM) mikrografar viste ei blanding av store agglomerat og individuelle NP i suspensjonen, og den påfølgjande bildeanalysen gav ein nanopartikkelstørrelse på 5 ± 1,4 nm.

I 96 timars eksponeringsstudiar i MHRW ved pH 7,1-7,4, vart 100% mortalitet observert ved 277 µM UO_2^{2+} og ved 1100 µM UO_2 NP. I UO_2^{2+} eksponeringsstudien var det ein signifikant reduksjon i reproduksjon og vekst ved 62 µM og høgare, men det var ingen endring i fruktbarheit. I UO_2 NP eksponeringsstudien var det ein signifikant reduksjon i vekst ved 140 µM og høgare, og i reproduksjon ved 240 µM og høgare. Ved 460 µM var fruktbarheit redusert til 0%. Nematodar eksponert for 240 µM hadde også eit uforholdsmessig stort munnparti, og hovne og misdanna tarmar. Regresjonsanalyse av eksponeringskonsentrasjon og effekt på reproduksjon viste at dose-responsen frå UO_2^{2+} var dobbelt så stor som den for UO_2 NP. Vidare var 10% effektkonsentrasjon (EC_{10}) og 50% effektkonsentrasjon (EC_{50}) mange gongar større for nanopartiklane enn for ionene. Dermed vart det konkludert med at UO_2^{2+} meir toksisk for nematodane enn UO_2 NP.

Fullstendig opptak og gjenværande U etter depurering vart undersøkt i nematodar eksponert for UO_2^{2+}og UO_2 NP. Induktivt kopla plasma massespektrometri (ICP-MS) målingar viste eit høgare opptak og retensjon i nematodar eksponert for UO_2 NP enn UO_2^{2+}. Det vil sei at sjølv om UO_2 NP har ein lågare spesifikk toksisitet, kan utslepp føre til bioamplifikasjon i miljøet.

Reaktiv oksygen specie (ROS) produksjon vart undersøkt som ein mogleg toksisk verkemekanisme (MOA) ved bruk at transgene stammar av *C. elegans* og fluorescensmikroskopi. I SOD-1 reporterstammen var det ein svak oppregulering av *sod-1* genet, som berre var signifikant i nematodar eksponsert for UO_2 NP. Derimot gav analyse av biosensorstammane Hyper og GRX ingen gyldige resultat, og dette temaet burde derfor undersøkast nøyare i framtidige studiar.

List of abbreviations

cpYFP	Circularly permuted yellow fluorescent protein
ddH_2O	Double-distilled water
DLS	Dynamic light scattering
DU	Depleted uranium
EC	Effect concentration
GFP	Green fluorescent protein
GRX	*C. elegans* biosensor strain jrIs2[Prpl-17∷Grx1-roGFP2]
GSH	Glutathione
GSSG	Glutathione disulfide
HSD	Honestly Significant difference
HyPer	*C. elegans* biosensor strain jrIs1[Prpl-17 ∷ Hyper]
ICP-MS	Inductively coupled plasma mass spectrometry
LB	Lysogeny broth
MHRW	Moderately hard reconstituted water
MOA	Mechanism of action
N2	Wild type Bristol *C. elegans* strain
NGM	Nematode growth media
NP	Nanoparticle
ROS	Reactive oxygen species
SD	Standard deviation
SOD	Superoxide dismutase
SOD-1	*C. elegans* reporter strain GA508 wuls54[pPD95.77 sod∷1GFP, rol-6(su1006)]
TEM	Transmission electron microscopy

Table of contents

1 Introduction

Toxicology is defined as the study of the harmful effects of chemical, physical and biological agents to organisms (Walker et al., 2012). Of central importance in this field is the relationship between the toxicant exposure dose and the induced biological response, meaning different substances are toxic at different concentrations (Walker et al., 2012). However, of equal or in some instances greater importance, is the specie of the toxicant. Certain elements that are considered harmless in some circumstances, may become lethal under other chemical conditions, such as changes pH or ionic strength (VanLoon and Duffy, 2011). With the surge of interest in nanotechnology, there have been concerns of adverse biological effects specific to nanoparticles (NPs), which has led to the emergence of nanotoxicology as a sub-field of toxicology (Donaldson, 2004).

Uranium (U) is a dense metal, which has seen extensive military- and civilian use. The element is most known for its use as fuel in nuclear reactors, as uranium enriched in the ^{235}U isotope is fissile (Choppin et al., 2014). While the radiotoxicity of the element is primarily dependent on the ^{235}U isotope, uranium is an inherently toxic chemical (Choppin et al., 2014). Organs retention and toxicity are both dependent on the chemical speciation and physio-chemical form (Guéguen et al., 2017).

Recently, methods for synthesizing uranium nanoparticles (U NPs) have been developed for the purpose of nanomedicine, electronics, and nuclear power (Hudry et al., 2014, Abostate et al., 2018, Čuba et al., 2014). However, today a considerable amount of anthropogenic U NPs are released incidentally as aerosols under high temperature conditions, such as DU projectiles fragmenting and igniting on impact (RSC, 2001). Uranium particles of varying sizes have been reported in military conflict zones, surrounding plane crash sites, and released from the production of nuclear fuel (Danesi et al., 2003, Salbu et al., 2005, Chazel et al., 2000, Uijt De Haag et al., 2000). Furthermore, high concentrations of U is released into waters by leaching from mine tailings and phosphate fertilizers (Choppin et al., 2014, Ahmed et al., 2014). Uranium released into the environment could cause harmful effects in both humans and other organisms. To limit these effects, studies on the environmental fate, and toxic mechanisms of U are needed (Walker et al., 2012).

While a significant number of studies have addressed toxic properties of uranium, few have investigated the toxicity of U NPs. Due to their small size and high surface to volume ratio, NPs are known to be highly reactive (De Matteis and Rinaldi, 2018). Thus, the toxic properties of NPs are dependent on chemical composition, as well as their physio-chemical properties, and characterization of these properties is an important prerequisite to fully understanding toxic mechanisms.

The nematode *Caenorhabditis elegans* has previously been used as a model organism in toxicology studies to assess the toxicity of U and other heavy metals (Dutilleul et al., 2013, Shen et al., 2009, Swain et al., 2004). It is found in many parts of the world, often inhabiting soil, making it prone to uranium both in the soil itself, and from ambient waters (Altun and Hall, 2012, Danesi et al., 2003, Walker et al., 2012).

In this work the size and surface charge of UO_2 NPs produced by photo-induced precipitation and heat treatment were characterized. The toxicity of the UO_2 NPs was compared to the toxicity of depleted uranium in the form of uranyl (UO_2^{2+}) in the nematode *C. elegans*. Three hypotheses were postulated:

I) UO_2 NPs are less toxic to *C. elegans* than UO_2^{2+}

II) UO_2 NPs and UO_2^{2+} cause toxic effects through the production of ROS

III) UO_2 NPs are less bioavailable than UO_2^{2+}

2 Theory

2.1 Uranium

Uranium is in the actinide group of elements and is characterized by its pyrophoric properties and high mass, with it being the heaviest naturally occurring element on earth. It can exist in oxidation states +3 through +6, with +6 being the most stable in oxic waters (Choppin et al., 2014). Uranium comprises 3-4 ppm of the earth's crust, which is roughly the same as for arsenic and boron. Natural U is composed of ^{238}U (~99.2745%), ^{235}U (~0.72%) and ^{234}U (~0.0055%) produced from the ^{238}U decay chain (figure 2.1.1). Enriched U is produced by separating the isotopes, removing part of the ^{238}U, which result in a much higher content of ^{235}U (anywhere from 2% to 90%). ^{235}U is fissile and is therefore often used in nuclear reactors. The byproduct from the enrichment process is commonly called depleted uranium (DU) and consists of an even larger part ^{238}U (~99,7%). DU has both military and civilian application, such as armor-penetrating munitions, trim weights in airplanes, and as radiation shielding, due to its high density. In 2010 the worldwide production of uranium from mining was 506 kton, and the extensive use may lead to increased environmental concentrations (Choppin et al., 2014).

Waterborne U has several anthropogenic and natural sources. Tailings from uranium mining may leach into local streams (Choppin et al., 2014). Increased U-levels has been reported in both soil and waters near agricultural areas where phosphate fertilizers have been used due to a natural content of U in phosphate minerals (Ahmed et al., 2014, Bigalke et al., 2018). Natural U can also be mobilized and leach into waters from weathering minerals (Wu et al., 2019). Furthermore, oxidizing agents such as nitrate which is used in fertilizers, can enhance mobilization of U species from minerals (Banning et al., 2013).

The most abundant species of uranium in aquatic environments is the uranyl ion ($U(VI)O_2^{2+}$), which forms strong complexes with carbonate (CO_3^{2-}) (Choppin et al., 2014). At higher pH negatively charged uranyl compounds are formed (see figure 2.1), which means high mobility in water, but low adsorption to cell membranes leading to low bioavailability (Fortin et al., 2004, Zeman et al., 2008). Bioavailability is also dependent on the presence of ligands like phosphate and hydroxyl, meaning that the toxicity of uranyl is highly dependent on complexation and pH (Hyne et al., 1992, Bird, 2012)

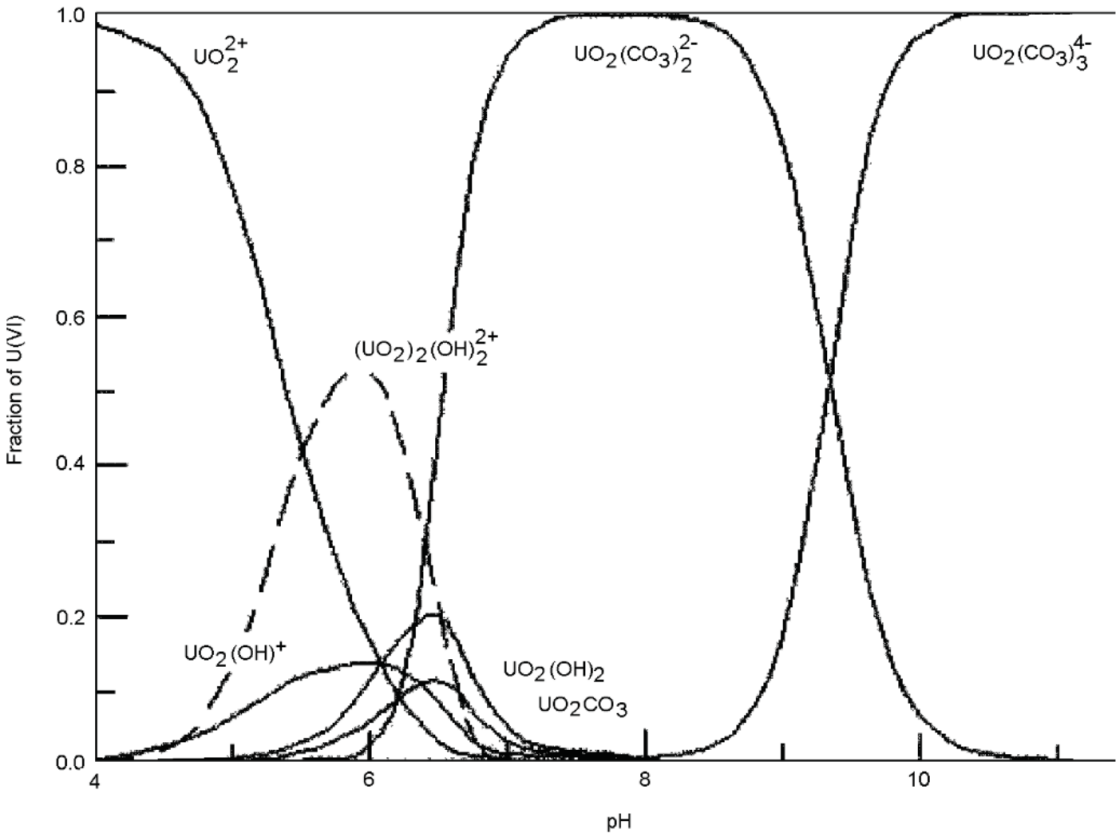

Figure 2.1: Uranyl speciation as a function of pH in oxic waters. Adapted from (Choppin, 2007)

During fires, micron to nanometer U particles may be released from bulk U. U- particles of varying sizes has been found in areas of military conflict where DU- armor penetrating munition had been utilized (Danesi et al., 2003, Salbu et al., 2005). Such particles are formed and released as a result of the high temperature of the impact, as U is pyrophoric (Choppin et al., 2014, RSC, 2001). Following the Boeing 747 cargo plane crashed in Amsterdam in the Netherlands, the 150 kg uranium trim weight was found to be missing. The U was assumed to have been oxidized in the fire and dispersed into the atmosphere (Uijt De Haag et al., 2000). When in the environment, Tetravalent U from uranium dioxide ($U(IV)O_2$) may be oxidized into UO_2^{2+} by air, releasing ions (Choppin et al., 2014).

Collectively the environmental release of U from nuclear industry, military activity, weathering and agriculture is substantial and increased concentrations may lead to adverse effects in humans and other organisms.

2.1.1 Radioactive traits of uranium-238

All isotopes of U are unstable, meaning they undergo radioactive disintegration. In the case of ^{235}U and ^{238}U this happens by α-decay (see figure 2.1.1). This type of ionizing radiation, which consists of ^{4}He-nuclei, only travels a few centimeters in air, and may be stopped by a thin sheet of paper. However if the radiating source is ingested and enters the cells it has the potential to cause severe damages. α-radiation has a high linear energy transfer, meaning it deposits a lot of energy in a small area and can cause dense track of ionizations. This way it has the potential to generate reactive oxygen species (ROS) and damage DNA (Choppin et al., 2014).

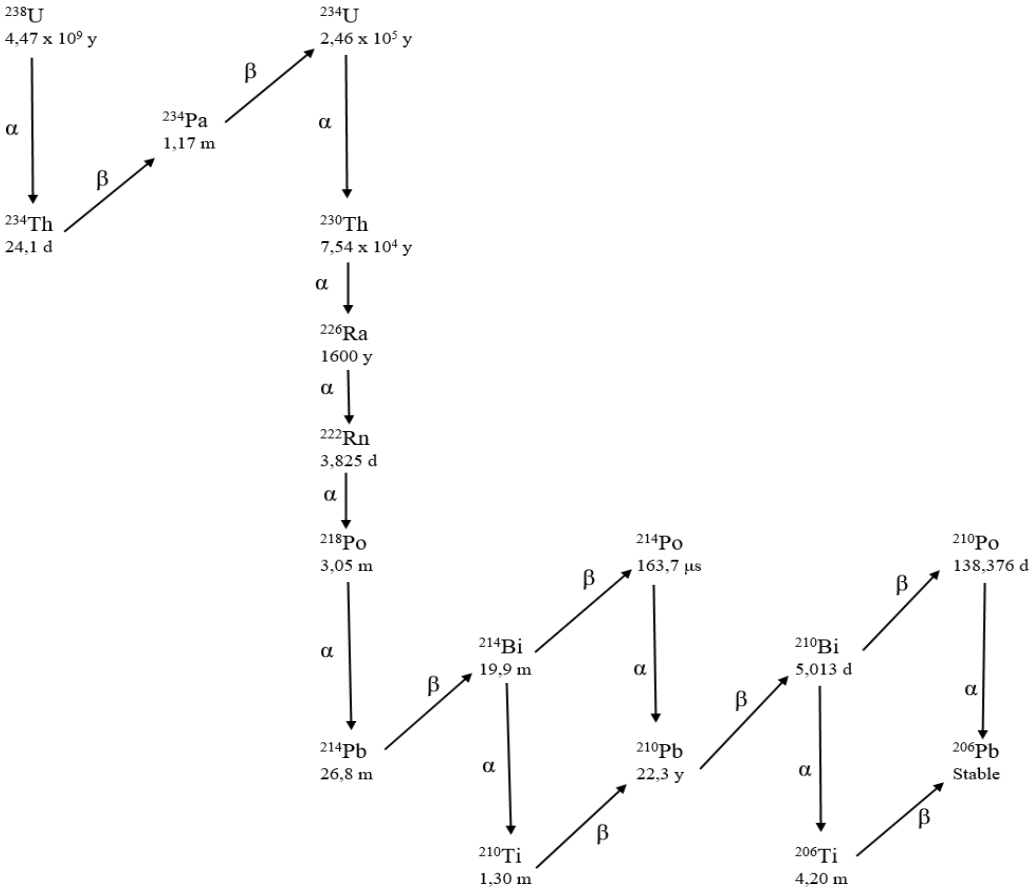

Figure 2.1.1: U-238 decay series. Decay mode is given as either α- or β-decay. Radioactive half-life for each isotope is given in years (y), days (d), hours (h), or seconds (s). Adapted from Choppin et al. (2014).

By exposing human osteoblast cells to different U isotopes, Miller et al. (2002) showed that neoplastic transformation was caused in an activity-dependent manner. In the experiment ^{238}U showed a relatively low specific activity and yielded a low transformation rate compared to ^{235}U. With a very long half-life of 4.47 x 10^9 years, ^{238}U is considered to be a weak α-emitter and toxicity is mostly attributed to its chemical properties (Choppin et al., 2014).

2.1.2 Uranium toxicity

A range of studies have been conducted to uncover the toxic effects of U. The bones and kidneys are generally considered to be the main accumulation sites for U compounds (Guéguen et al., 2017). During long term chronic exposures U can accumulate in bones by displacing calcium (Pellmar, 1999, Arsenault and Hunziker, 1988). Hurault et al. (2019) reported that osteocytes, cells involved in bone remodeling, displayed a decrease in mineralization function and cell viability when exposed to U(VI). Zamora (1998) reported that elevated levels of U in groundwater supplies interfered with kidney function and caused renal damage following long-term ingestion. Uranium has also showed the ability to be transported into the brain and cause neurological damage, possibly through lipid oxidation, in rodents. (Barber et al., 2007, Briner and Murray, 2005, Lemercier et al., 2003).

Several of the toxicological effects of uranium are linked to the production of ROS. Uranium has been shown to produce ROS in rat lung cells, oxidizing glutathione, decreasing the antioxidant potential (Betteridge, 2000), and subsequently causing oxidative damage to DNA (Periyakaruppan et al., 2007). Serial analysis of gene expression has shown an upregulation of genes related to oxidative stress, inflammation, and apoptosis in the kidneys (Taulan et al., 2006, Taulan et al., 2004).. The proposed mechanism for ROS-production is similar to a Fenton type reaction where uranyl catalyze the formation of hydroxyl radical (OH·) from hydrogen peroxide (H_2O_2, see equation 1 & 2)(Hamilton et al., 1997).

$$UO_2^{2+} + 2H^+ + 2e^- \rightarrow UO^{2+} + H_2O \qquad (1)$$

$$UO^{2+} + H_2O_2 \rightarrow UO_2^{2+} + OH\cdot + H^+ \qquad (2)$$

A range of studies have investigated the effect of U in *C. elegans*. Goussen et al. (2015) reported that nematodes exposed to U displayed decreased growth and reproduction. The results supported the hypothesis that this was caused by damage to the intestines leading to a decreased ability to acquire energy from food (Massarin et al., 2011). Lu et al. (2020) reported no effect on reproduction or lifespan in nematodes exposed to 1mM U. The exposure did, however, lead to the degradation of dopaminergic neurons and promoted the increase of α-synuclein aggregation and dopaminergic neurotoxicity. It also reduced the expression of *ctl-1, ctl-2 ctl-3, gst-7* and *gst-10*. Dutilleul et al. (2013) reported that in a multigenerational exposure, U had a negative effect on survival, generation time, brood size, body length, and body bend activity in *C. elegans*. On the lower concentrations these effects were reduced in consecutive generations, likely due to adaptative processes. All of the aforementioned studies were performed on agar plates, and none report exposure pH.

A notable method *C. elegans* has for heavy metal detoxification are metallothioneins, which are present in the intestine of the nematode (Altun and Hall, 2012). Metallothioneins are low molecular weight, cysteine-rich proteins that have metal-binding and redox capabilities (Coyle et al., 2002). The metallothioneine forms metal-thiolate complexes with the metallic toxicants rendering them inert. Using knockout-strains in an uranium exposure, Jiang et al. (2009) showed that metallothioneins slightly reduced mortality, while accumulating DU. The study suggested that out of the two isoforms present in the nematode, metallothionein-1 binds the U within the cell, while metallothionein-2 is involved in the transport of the U out of the cell.

2.1.3 Uranium nanoparticles

Nanoparticles (NPs) are generally defined as small particles, which are less than 100 nm in at least one dimension (Walker et al., 2012). Particles in this size range are shown to have the ability to enter cells through endocytosis (Rejman et al., 2004). Interestingly, some nanoparticles has shown an increased ability to cause oxidative stress, inflammation and genotoxic effects compared to other species of the same chemical (Brown, 2000, Lindberg et al., 2012).

In contrast to other chemical toxicants, the toxicity of NPs is dependent not only on the chemical composition of the particle, but also physical properties (De Matteis and Rinaldi, 2018). Due to their small size they have a large surface to volume ratio, rendering them more biologically active than larger-sized particles (Chazel et al., 1998, Platel et al., 2016). Size, shape, charge, and surface chemistry of the particles determine their rate of agglomeration and ability to enter cells, as well as their ability to generate ROS, and dissociate and release ions (De Matteis and Rinaldi, 2018, Platel et al., 2016, Nowack and Bucheli, 2007).

The physio-chemical properties of NPs are not only dependent on the particles themselves, but also their local environment (Pfeiffer et al., 2014). NPs with a surface charge of ±40 will normally make up a suspension with good stability due to electrostatic repulsion (Zhang et al., 2012, Kumar and Dixit, 2017). However, ions present in the liquid may dissipate the repulsion and promote agglomeration, potentially reducing the toxicity of the NPs. It is important to keep this in mind when assessing toxicity through liquid exposure studies. Exposure media such as M9 and K-medium have relatively high ionic strength. This is not expected under realistic soil pore water conditions, and exposure media with a lower ionic strength should be used instead (Tyne et al., 2013).

The particles used in the present work were UO_2 nanoparticles. The preparation of these particular particles involve a combination of photo-induced precipitation, and subsequent heat-treatment in order to obtain the crystalline oxides (Čuba et al., 2014, Pavelková et al., 2016, Pavelková et al., 2013). The resulting particles have a diameter between 3 and 15 nm and may have applications within the production of nuclear fuel.

Only a limited amount of studies have investigated the toxicity of U NPs. When insoluble U compounds are inhaled, the lungs are generally considered to be the primary target both in terms of entrance and accumulation (Guéguen et al., 2017). A study on U_3O_8 particles showed that absorption from the trachea to the blood in rats increased proportionally with decreasing particle surface area (Chazel et al., 1998). Petitot et al. (2013) showed that UO_2 NPs inhaled by rats were deposited in the respiratory tracts and lungs before they were translocated to the kidneys and bones. Liu et al. (2015) reported that the uranyl from a mixed U-species exposure was transformed into uranyl phosphate particles, which lead to uptake and apoptosis in rat hepatic BRL cell.

After inhalation and internalization these particles may cause harm in cells. As previously mentioned, a common feature among NPs is their ability to produce ROS due to their high surface area and the presence of oxidants and functional groups on the particle surface (Risom et al., 2005, Knaapen et al., 2004). These types of reactive compounds may have a negative impact on cell function when allowed to accumulate.

2.1.4 Reactive oxygen species and oxidative stress

Reactive oxygen species are highly reactive chemical species containing oxygen (Elliot and Elliot, 2009). Certain types are chemical radicals, which contain unpaired electrons, like the hydroxyl radical (·OH) and superoxide ($\cdot O_2^-$). Meanwhile, hydrogen peroxide (H_2O_2) is a reactive oxygen specie that has the ability to form ·OH. Within the cell there is a certain amount of ROS produced in the mitochondria due to incomplete reduction of oxygen. Increased ROS levels can also be the consequence of external stressors. Exogenous ROS-generating stressors include ionizing radiation, and xenobiotics such as heavy metals and chemical radicals (Elliot and Elliot, 2009, Hamilton et al., 1997). When cell is unable to maintain a low concentration of ROS due to a disturbance in the balance between its production and antioxidant defenses, oxidative stress may occur (Betteridge, 2000). Due to their highly reactive nature, ROS react quickly with random molecules in the cell, which can lead to free radical chain reactions and damage different biological constituents such as macromolecules (i.e. lipids, protein and DNA) (Elliot and Elliot, 2009, Betteridge, 2000).

A primary defense mechanism in the cell for removal of ROS is the superoxide dismutase (SOD) enzyme, which catalyzes the dismutation of O_2^{2-} to O_2 and H_2O_2 (Equation 3). H_2O_2 is a source for ·OH, which is still harmful to the cell if not sequestered properly. In the cell H_2O_2 is reduced to H_2O either by catalase or peroxidase enzymes. The latter require use of the antioxidant glutathione (GSH, see equation 4). GSH is oxidized into glutathione disulfide (GSSG), which is reduced by hydrogen nicotinamide adenine dinucleotide phosphate (NADPH) catalyzed by glutathione reductase (Equation 5). This way glutathione is recycled (Elliot and Elliot, 2009).

$$2O_2^- + 2H^+ \rightarrow H_2O_2 + O_2 \qquad (3)$$

$$H_2O_2 + 2GSH \rightarrow 2H_20 + GSSG \qquad (4)$$

$$GSSG + NADPH + H^+ \rightarrow 2GSH + NADP^+ \qquad (5)$$

Since reactions involved in free radical damage occur almost instantaneously, ROS cannot be measured directly and must be assessed through biomarkers in *in vitro* experiments (Betteridge, 2000). Potentially, biomarkers could be measured *in vivo,* given the right model organism.

2.2 *Caenorhabditis elegans*

Caenorhabditis elegans is a non-parasitic roundworm that is usually found in temperate soil environments, but also in rotting fruit and vegetable matter, feeding mainly on bacteria (Riddle et al., 1997, Altun and Hall, 2012). This is an important model system for biological research: its complete cell lineage is known and it was the first multicellular organism, which genome was sequenced (The C. elegans Sequencing Consortium, 1998, Altun and Hall, 2012).

The life cycle of *C.* elegans is shown in figure 2.2. After hatching, the nematode develops through four larval stages (L1-L4) before reaching adulthood (Altun and Hall, 2012).The end of each larval stage is marked by molting and development can be finished within three days given the optimal temperature, chemical conditions, and sufficient access to food. If the embryos hatch in the absence of food, they arrest development and can survive for 6-10 days before returning to normal development, given that food becomes available. If unfavorable conditions persist, L1 nematodes may enter the Dauer stage. Environmental factors such as high temperatures, insufficient food, or high population density (indicated by pheromone production) all act as triggers that cause the nematodes to enter this arrested state. The Dauer larvae are able to survive in tough conditions for as long as four months. If conditions improve, development may resume and they enter the L4 stage (Altun and Hall, 2012). The adult hermaphrodites can produce up to approximately 300 offspring by self-fertilizing, or up to 1400 offspring in the presence of males, which, under normal circumstances only makes up about 0.1% of the population (Altun and Hall, 2012). The adult nematode consume several million bacteria (*Escherichia coli*) each day, but may also ingest particles up to 3 μm in diameter (Ghafouri and McGhee, 2007, Kiyama et al., 2012). The intestinal content has a residence time of less than two minutes, thus bacteria and foreign matter are quickly excreted.

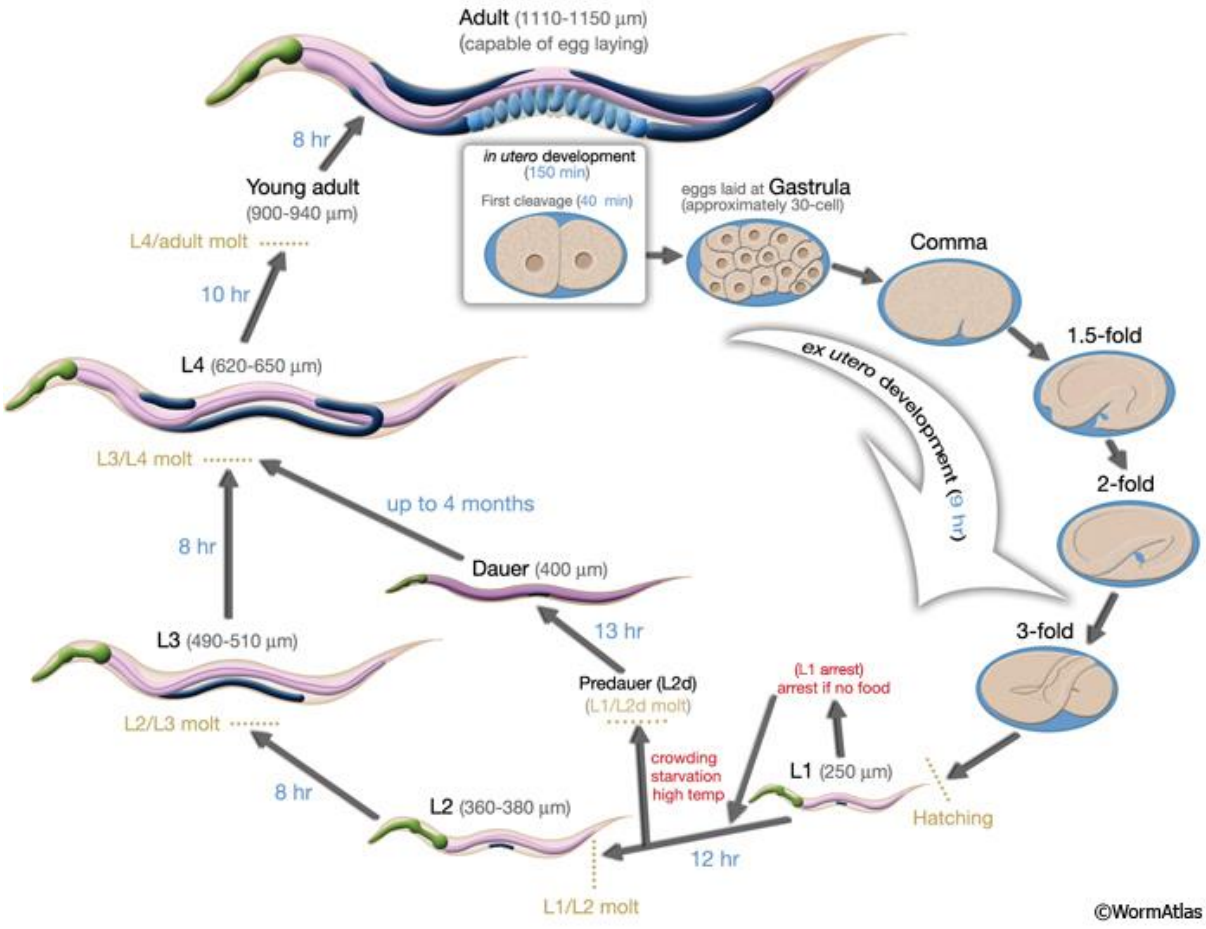

Figure 2.2: The life cycle of *C. elegans* at 22^{o} C. Adapted from Altun and Hall (2012).

The nematode has been used as model organisms since the 1970s when their potential was first realized (Brenner, 1974). Several aspects make them well suited as model organisms: They have a relatively short reproductive life cycle, meaning that toxicity tests can be less time consuming (Altun and Hall, 2012). This can be very useful for nanotoxicology studies due to NPs tendency to agglomerate and dissolve over time (Handy et al., 2012). When reaching their adult stage they are about 1 mm in length meaning that exposure studies can be conducted in 1 mL exposure wells. Their small size combined with their transparent body make them practical to study through microscopy methods and especially suitable for fluorescence analysis. Also, they are a very well studied biological model, which means that normal development is predictable (Altun and Hall, 2012).

In toxicological studies, using a self-fertilizing culture of the N2 Bristol strain of *C. elegans* means that there is little variation between individuals. Alkaline hypochlorite treatment yields an age-synchronized L1 larvae cultures, which also helps reduce variation between individuals. This is useful when measuring toxicological endpoints such as decreased reproduction and fertility, reduced growth, and mortality.

C. elegans is amenable to genetic modification and several transgenic strains that are useful for assessing toxicological endpoints have been developed. Common for the ones used in the current study is the utilization of fluorescent proteins as reporters for various stimuli. One of them is the GA508 wuls54[pPD95.77 sod1::GFP, rol-6(su1006)] (SOD-1) reporter strain where a *sod-1*::*gfp* transgene is integrated in the *rol-6* locus (Doonan et al., 2008). *C. elegans* has five different SOD isoforms, of which *sod-1* and *sod-5* are expressed in the cytosol of the cell. When the cell experiences elevated levels of ROS in the form of O_2^- in the cytosol or the mitochondrial intermembrane space, the *sod-1* gene is expressed. In GA508, the *gfp* is coexpressed with *sod-1*. This means that the green fluorescent protein (GFP) signal can be used as a biomarker for increased O_2^--concentrations.

As a result of the transgene being integrated in the *rol-6* locus, the SOD-1 strain move forward in a rolling motion like a screw instead of the sliding motion of the wild type (Oeda, 2001). Rollers like this can excise the transgene via homologous recombination (Elliot and Elliot, 2009), thus losing their fluorescence properties.

Another transgenic strain is the HyPer biosensor (Belousov et al., 2006, Back et al., 2012) Normally, OxyR works as a H_2O_2 sensitive transcription factor for *E. Coli*. In the case of HyPer, the gene encoding OxyR has been fused with a modified cpYFP gene encoding a circularly permuted yellow fluorescent protein (cpYFP) (Belousov et al., 2006, Back et al., 2012). When H_2O_2 is present, it generates a disulfide bridge in the OxyR, inducing a change in fluorescent properties. Thus HyPer can be used as a proxy for changes in cellular H_2O_2 levels.

The GRX biosensor strain of *C. elegans* is modified with the human glutaredoxin-1 fused with redox sensitive green fluorescent protein Grx1-roGFP2 (GRX) (Gutscher et al., 2008, Back et al., 2012). The roGFP2 is sensitive to the GSH/GSSG redox state (See equation 5) and will emit different wavelengths when reduced or oxidized. Grx1 works as a catalyzer for the GSH/GSSG equilibrium. The GRX strain functions as a biosensor for the cellular redox state *in vivo* and as a proxy to assess oxidative stress development (Gutscher et al., 2008, Back et al., 2012).

2.3 Optical microscopy

2.3.1 Stereo microscopy

Optical microscopes, or light microscopes typically utilizes a light source and lenses to perform low powered magnification. Also, in a stereo microscope there are two separate eyepieces, creating a 3D-effect when observing a specimen.

Although the *C. elegans* nematode has an ideal size for being studied through such a microscope, they are transparent, making them troublesome to study using typical bright-field microscopy due to little contrast in the light absorbed. When using phase-contrast microscopy, the phase of the observed light is shifted by a lens, which makes it possible to see the diffracted light instead of the light unabsorbed by the specimen. This makes it easier to study the nematodes.

Another way to make the nematodes easier to view is by staining them. Using Rose Bengal (4,5,6,7-tetrachloro-2’,4’,5’,7’-tetraiodofluorescein) for staining gives the nematodes a fuchsia-color, which makes especially the L1 larvae a lot easier to view (Murphy and Davidson, 2013).

2.3.2 Fluorescence microscopy

When an atom or molecule is hit by a photon, the energy is transferred to electrons, which become excited to a higher and unstable energy level. When they return to their ground state the energy is released in the form of a new photon with less energy and, therefore, a lower wavelength. This shift in wavelength, called Stokes shift, makes it possible to differentiate the fluoresced light from the ingoing light. In fluorescence microscopy, a high intensity light source is used to excite any fluorescent substances in the specimen and it can be detected and quantified by measuring the emitted light (Sanderson et al., 2014).

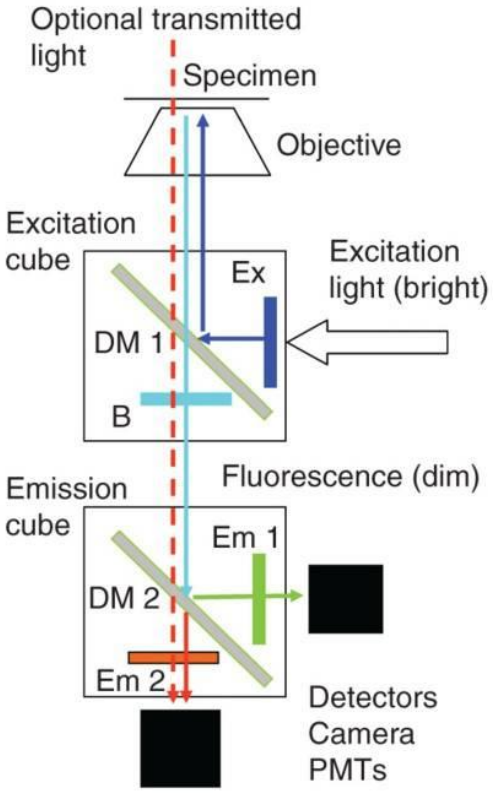

Figure 2.3.2: The basic light paths in a fluorescence microscope. Adapted from Sanderson et al. (2014).

A fluorescence microscope is similar to an optical microscope, but with a few modifications as shown in figure 2.3.2 (Sanderson et al., 2014). In addition to the regular light source, there is a high intensity light source. In the case of the Leica DM 6B it is a laser followed by an excitation filter where only the desired wavelengths pass through, followed by dichroic mirror that reflects the beam onto the specimen. Any emitted light caused by fluorescence will then pass through an emission filter before it is redirected to the detector camera by a prism. The information picked up by the detector is then used to produce an image displaying fluorescence in the specimen.

2.4 Dynamic light scattering

Dynamic light scattering (DLS) is a method for determining diffusion behavior and size distribution of macromolecules in a solution (Stetefeld et al., 2016). The Zetasizer Nano ZS (Malvern Instruments, 2013) is comprised of a light source in the form of a laser, a sample holder and a photodetector. When light hits the particles it is scattered in multiple directions. Due to the Brownian motion of the particles the intensity of the scattered light fluctuates, and this changing intensity is recorded by the detector. These fluctuations are then related to the hydrodynamic radius and size of the particle.

In addition to the mean value for size, the Zetasizer Nano ZS also gives a polydispersity index (PDI). This number is used to determine whether the sample is mono- or polydispersed (i.e. if the particles are all one size, or if there is a range of different sizes), where a PDI < 0.1 is considered a reasonably narrow size distribution (Malvern Instruments, 2013). The value is also used as an indicator of particle stability within the suspension, where a lower PDI equals a higher stability (Masarudin et al., 2015)

When a charged particle is suspended in a solution it will attract counterions that concentrate near the particle surface (figure 2.6). The inner layer of ions, known as the Stern layer, is comprised of strongly bound ions that travel with the particle. Ions further away from the surface are more loosely bound and make up the diffuse layer. The boundary between these two layers is called the slipping plane and the electrical potential that exists here is known as the Zeta potential.

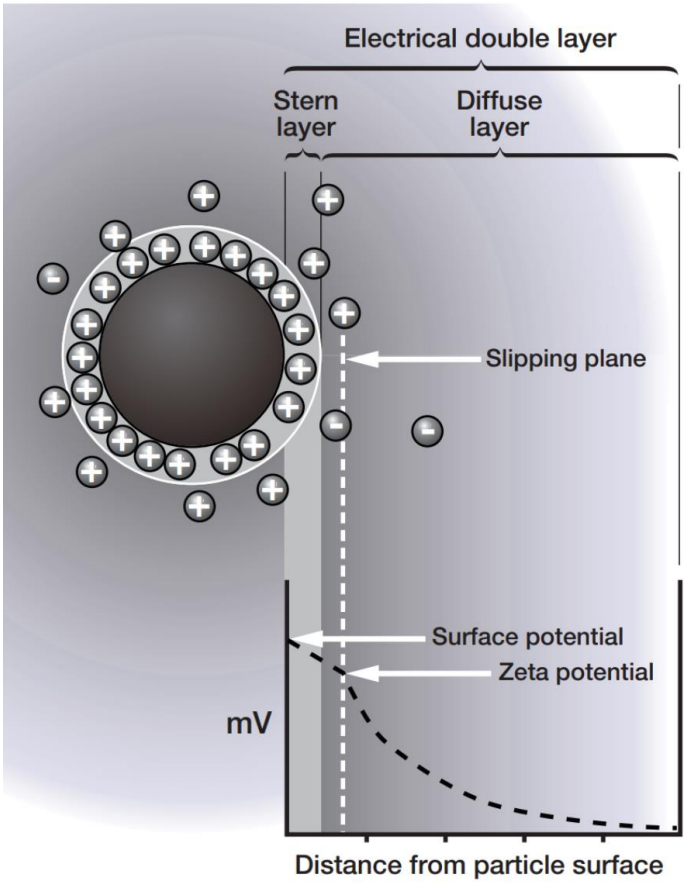

Figure 2.6: The electrical double layer surrounding a charged particle. Adapted from Malvern Instruments (2013).

When an electrical field is applied to the solution, the particles will move towards the opposite charge. The velocity of the moving particles, commonly known as electrophoretic mobility, can then be used to determine the zeta potential using the Henry equation:

$$U_E = \frac{2\epsilon z f(Ka)}{3\eta} \qquad (6)$$

where U_E is the electrophoretic mobility, ϵ is the dielectric constant of the medium, z is the zeta potential, f(Ka) is Henry's function, and η is the viscosity of the medium.

One way to measure the electrophoretic mobility of the particles is laser doppler velocimetry. Similarly to the DLS the particles are illuminated by a laser and incoming light is scattered. The incident beam which passes through the sample is combined with a reference beam, producing a fluctuating intensity signal. The fluctuation is proportional to the speed of the particles and can be used to determine the zeta potential of the nanoparticles (Malvern Instruments, 2013).

There are some drawbacks to DLS-analysis. It is sensitive to the presence of larger particles, and due to its low peak resolution it often cannot differentiate between highly similar molecules. In the case of polydisperse solutions, a more precise method may be necessary.

2.5 Transmission electron microscopy

As the name implies, in transmission electron microscopy (TEM) an electron beam is used to create an image of the sample instead of light (Williams and Carter, 2009). While a light microscope is limited by the wavelength of visible light, TEM is able to produce images with a much higher resolution with an electron beam. The wavelength (λ) of an electron is determined using the de Broglie equation (Williams and Carter, 2009):

$$\lambda = \frac{h}{p} \qquad (7)$$

where h is Planck's constant, and p is the momentum of the electron.

The wavelength of a 100 keV electron is 0.00370 nm, which gives the TEM a much better resolution than that of a typical light microscope (about 300 nm). TEM is usually used to image objects in the nano regime (<100 nm), making it useful for studying nanoparticles (Williams and Carter, 2009).

In principal, the TEM is comprised of an electron gun, followed by a series of magnetic condenser lenses, a sample holder and a detector. First, the electron beam is produced by a thermionic source. A tungsten filament is heated up to give the electrons sufficient energy to leak out. Then, series of magnetic condenser lenses accelerate the electrons and helps focus the beam onto the specimen, which is mounted on a copper grid. Then, depending on the density and thickness of the specimen, the electrons are either stopped by or pass through it. The transmitted electrons are then collected onto a fluorescent screen or a charge-coupled device. This information is then interpreted by the software and an image of the specimen is produced.

There are, however, a few limitations to TEM (Williams and Carter, 2009). As a consequence of the high resolution, the sampling size of TEM is limited. This means that only a small portion of the specimen may be studied at a time. When imaging 3D specimens, 2D images are produced. Thus, information about the shape of the specimen is limited to silhouettes (see figure 2.5). Also, the specimen has to be electron transparent, and specimens thinner than 100

nm should be used whenever possible. When preparing NP suspensions for TEM imaging, as well as when drying them on the copper grids, particles may agglomerate and create artefacts (see figure 2.5).

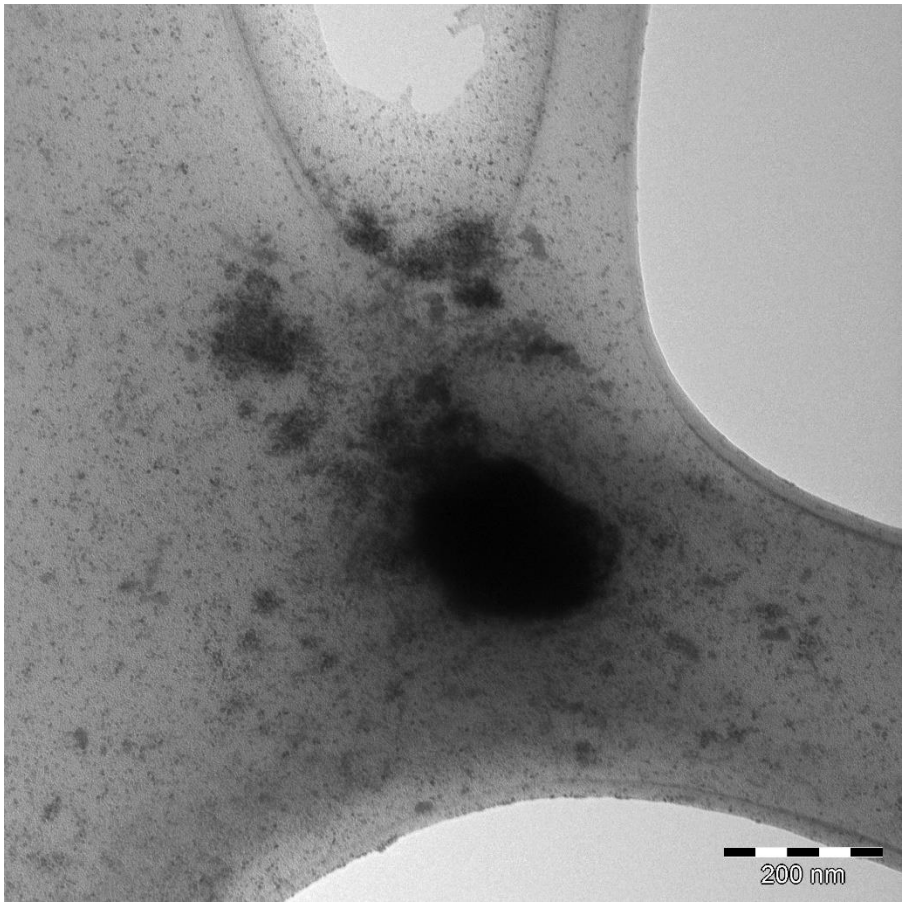

Figure 2.5: TEM image of UO_2 NPs on a copper grid with a perforated carbon. The NPs are only shown as black silhouettes, and a large agglomerate has formed in the center of the image.

2.6 Inductive coupled plasma mass spectrometry

Inductive coupled plasma mass spectrometry (ICP-MS) is an accurate and sensitive method for determining the chemical composition of a sample. The principles of ICP-MS are described by Skoog et al. (2018). The main components of the instrument are shown in figure 2.6.

After being inserted through the autosampler, the sample is sent through a nebulizer where it is converted into an aerosol. While the larger drops are removed as waste, droplets (< 10 μM) are lead into the torch. Here the argon plasma is first ignited by an electric spark and then maintained by radio frequent magnetic field causing argon ions to collide with each other, creating friction heat out to 10 000^{o} K. The sample is atomized and positive ions are created due to the high temperature. The content of the plasma is extracted through a water cooled nickel cone with a small orifice in its center. On the other side the pressure is less than 0.01 Pa. Here a series of lenses focus and accelerate positive ions into a beam while removing photons, and neutral and negative species.

The next part of the instrument are the mass filters. Here the ions are passed through the quadrupole, which consist of two pairs of connected electromagnetic rods. An alternating current accelerate the ions and depending on their mass/charge-ratio (m/z) they either pass through the quadrupole or they collide with the rods, and are thus filtered out. This way only compounds with a specific m/z reaches the detector. If the sample contains substances with a similar m/z to the analyte, gas flow may be added to the reaction cell. The reaction gas facilitates separation in the quadrupole by adding mass to the analyte or the interferences. This way many potential interferences may be removed.

Some instruments like the Agilent 8900 QQQ (triple quadrupole) also includes an additional quadrupole in front of the reaction cell (see figure 2.6). This makes it possible to remove much of the sample matrix before the reaction cell, ensuring that the gas flow only interacts with the analyte or the targeted interfering compound.

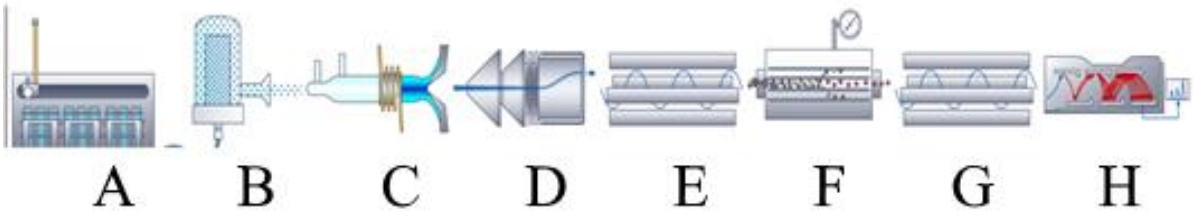

Figure 2.6: Main components of an ICP-MS instrument. Included are A) autosampler, B) nebulizer, C) plasma torch, D) sampling cone and lens system, E) and G) quadrupoles, F) reaction chamber (octupole), and H) discrete dynode detector. Note that there is an additional quadrupole placed in front of the reaction cell. Screenshot from Masshunter software (Agilent).

In the final step, the ions reach the discrete dynode detector. Here energetic ions collide with the dynode and knock loose electrons, which are attracted to the next dynode where more electrons are knocked loose. This chain reaction leads to a high number of electrons hitting the last dynode for each ion entering the detector, which provides a low detection limit. The resulting electrical signal is read as counts for each ion. The concentration is then determined by comparing the number of counts to a calibration curve made from standard solutions. In the case of elements where more than one isotope are present, total concentration has to be calculated from the isotope ratio since only one isotope is measured.

One benefit of measuring U-concentration with ICP-MS is that there are few spectral interferences. These types of interferences are divided into doubly charged ions, isobaric and polyatomic interferences (Skoog et al., 2018). Doubly charged ions are in this case ions with oxidation number 2 that also have twice the mass of the analyte and therefore the same m/z. With the high mass of ^{238}U, there are no elements, which have a mass that high. Isobaric interferences, which are isotopes of other elements with the same mass as the analyte, does not occur with ^{238}U since they all have short half-lives and do not exist naturally. Polyatomic interferences are polyatomic species that form in the plasma, in the matrix or in the atmosphere, and have the same mass as the analyte. For uranium these typically include $^{198}Hg^{40}Ar^{+}$, $^{198}Pt^{40}Ar^{+}$ and $^{202}Hg^{36}Ar^{+}$. However, mercury (Hg) and platina (Pt) are usually quite rare metals and are therefore not expected to cause any interference when working with nematodes.

Another typical Interference in ICP-MS are matrix effects. If the viscosity is higher in some samples the nebulization will be less efficient and there will be a reduction in analyte signal. Matrix effects can be minimized by dilution, and making sure that salt concentrations and pH is similar between samples. An easier way to deal with matrix effects is by using an internal standard. By adding a known concentration of an element with similar chemical properties as the analyte, preferably another isotope of the analyte, any loss of analyte can be accounted for.

In some cases ethanol is introduced into the plasma in order to enhance the analyte signal (Wiltsche et al., 2015). The mechanism behind this is thought mainly to be a combination of improved nebulization due to a change in viscosity, and carbon induced charge exchange reactions. This means that more sample reach the plasma torch, and that more of the analyte is ionized and is able to pass through the mass filters.

2.7 pH electrode

Ever since the 1930s, the most convenient method for determining pH has been through a pH electrode. The basic principle of a pH electrode is that pH is determined by measuring the difference in electric potential across a glass membrane separating the sample from a reference electrode. When the probe (see figure 2.7) is immersed in the sample solution, H^+ ions react with the glass membrane through ion-exchange. H^+ ions are then released internally and a potential is created across the membrane. The two reference electrodes act as electrical contacts with the solution, making it possible to measure this potential. (Skoog et al., 2018)

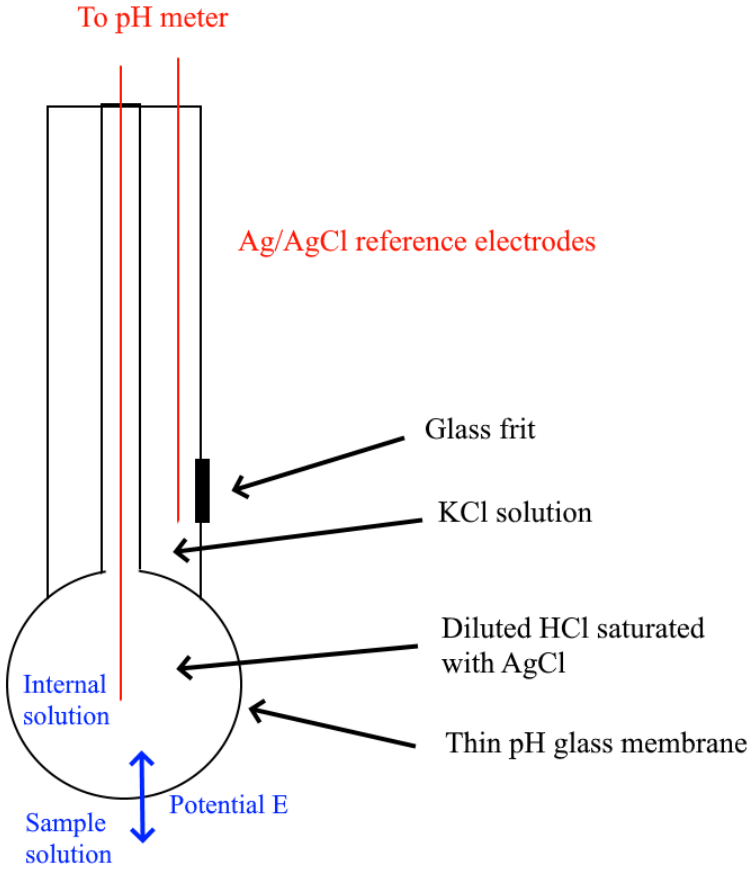

Figure 2.7: Schematic showing the main components of a combined pH electrode. Note that the pH of the internal solution should be known in order for the sample pH to be calculated. Adapted from Skoog et al. (2018).

When the electrical potential across the membrane (E) is known, pH in the sample is calculated by the pH meter using the Nernst equation (Skoog et al., 2018):

$$E = E_{Sample} - E_{Internal} = 0.0592\left(pH_{Internal} - pH_{Sample}\right) \qquad (8)$$

3 Materials and methods

3.1 Preparation of nanoparticle suspension

The NP suspension was prepared by weighing out approximately 11.3 mg aliquots of NPs in glass vials. Following this, 100 µL of NM-300KDIS Ag-dispersant (Frauenhofer IME) was added and the vial was swirled in order to coat as many NPs as possible before diluting to 10 mL with de-oxygenated double-distilled water (ddH_2O) water. The ddH_2O water was de-oxygenated in advance by placing it in a nitrogen tent and bubbling it for at least 30 minutes with nitrogen gas. The mixture was then sonicated using a Branson S-450 D sonicator with a 13 mm disruptor horn. The vial containing the suspension was placed in an ice bath, partially submerged, and held in place by use of a retort stand and clamps. The disruptor horn was placed into the suspension and, making sure it did not make contact with the glass vial, held in place using the retort stand. The NPs were then sonicated at 15% amplitude for 13 minutes. The disruptor horn was cleaned of U before and after each preparation by sonicating ethanol and then rinsing it with water.

In order to control the efficiency, a DLS analysis was performed immediately following the sonication. A 1 mL aliquot of the prepared NP suspension measured using a PN3702 Zetasizer Nano ZS (Malvern Panalytical). To ensure a consistent NP suspension, a size distribution of approximately 173 ± 8.2 nm was accepted.

3.2 Nanoparticle characterization

Nanoparticle zeta potential was determined by placing 1 ml of NP suspension in a folded capillary zeta cell (DTS10170, Malvern Panalytical), which was then measured using the Zetasizer Nano ZS. Afterwards the zeta cell was cleaned using ethanol and ddH_2O.

In order to get a more accurate estimate of NP size, 5 µL of NP suspension was air dried on a perforated carbon copper grid and imaged using a FEI Morgagni 268 TEM. Images were taken at 80 keV using 100-180x magnification.

TEM micrographs were analyzed using ImageJ. Making sure to avoid artefacts such as agglomerates, smaller areas of the image were selected and converted into binary images (see figure 3.2). Particle size was determined using the "analyse particles"-tool. In order to avoid measuring noise (i.e. small impurities in the image that are not really particles, but rather part of the background of the unedited image) in the image, the lower size limit was set to 4 nm.

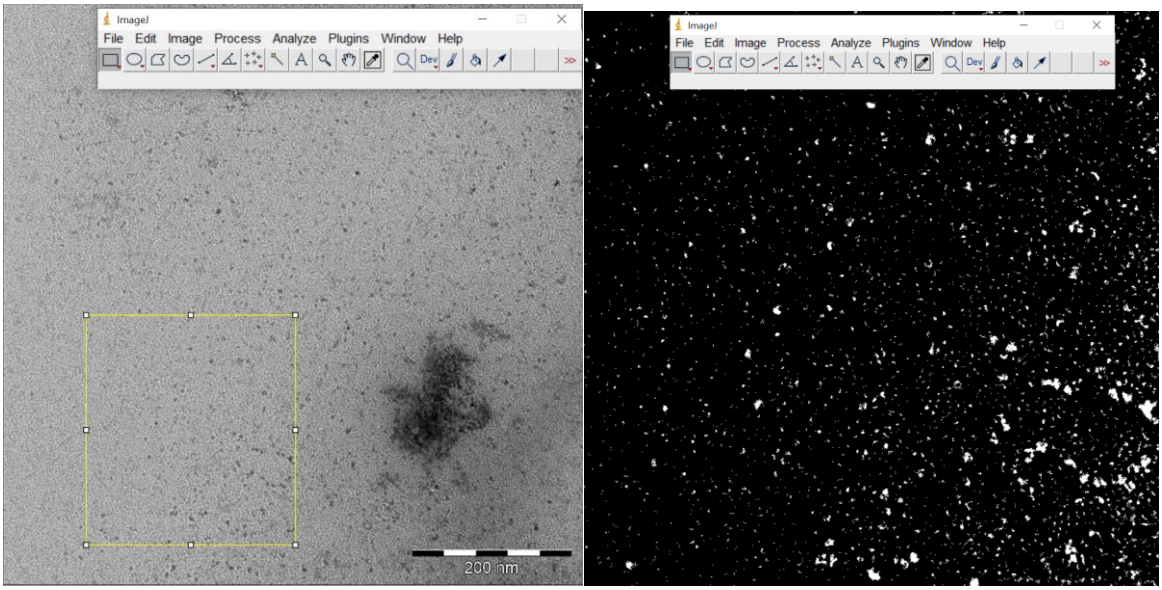

Figure 3.2: To the left: Picture taken with the TEM where an area has been selected for analysis (yellow square). To the right: binary image of the selected area created by setting a signal threshold. Thus, the nanoparticles are displayed as white objects on a black background.

The concentration of the NP suspension was determined by ICP-MS analysis. 100 µL of suspension was extracted from the prepared stock and collected in 15 ml falcon tubes. For digestion, 500 µL of concentrated HNO_3 was added to the sample and incubated at 90^o C for 2 hours. In order to reduce the acid concentration to 5% (v/v)HNO_3, samples were diluted to final volume 10 mL using MilliQ water. Further dilution was performed using 5% (w/w)HNO_3.

3.3 Fractionation

In order to characterize the behavior of the uranyl ions and U-NPs, uranium size fractions were investigated both at the beginning (T-0h) and the end (96h) of the exposure period. Thus, colloidal, suspended, and low molecular mass (LMM) U fractions were assessed. This was done for low, medium and high U concentration as well as control groups for both uranyl and NP exposure. Thus, it could be determined whether the U agglomerated or dissolved during the 96 hours.

The fractionation was performed immediately at T-0h and 96h to avoid any further change in U speciation. For each replicate 100 µL was extracted for ICP-MS measurements of total U-content. In order to decompose these samples, 500 µL concentrated HNO_3 was added to these samples and they were incubated at 90 °C for 2 hours. Afterwards they were diluted to 10 mL using MilliQ-water. The remaining volume of the wells were placed in separate Eppendorf tubes and centrifuged at 5000 g for 5 minutes. Then, 100 µL of the supernatant was sampled for ICP-MS measurement of suspended U-content, 500 µL of HNO_3 added, and they were decomposed at 90 ^{o}C for 2 hours. Finally, they were diluted to 10 mL using MilliQ-water. Before obtaining the LMM fraction, the 3 kDa filters were preconditioned using 200 µL of the remaining sample. After centrifuging for 10 minutes, the filtrate was discarded and the filters were placed in clean Eppendorf tubes. Then, 400 µL of sample was placed on top of the filter and the tubes were centrifuged at 14 000g for 30 minutes. The tubes were weighed so that the filtrate volume could be determined accurately. Afterwards they were dried and then resuspended in 1mL 5% (w/w) HNO_3. Due to the high sensitivity of the ICP-MS, if the expected U concentration in any of the samples were greater than 0.1 µM U they were diluted using 5% (w/w) HNO_3.

3.4 ICP-MS measurement

The uranium concentration in all samples was measured using an Agilent 8900 QQQ ICP-MS. The samples were placed in an Agilent ASX-500 autosampler which was connected to the ICP-MS. The calibration curve was made from a calibration blank and two calibration standard samples. The concentration of the first standard was decided depending on the expected U-content of the samples. The second standard was made by diluting the first standard ten times. In order to control the accuracy of the measurements, a certified standard was also measured. Indium-115 was added online as an internal standard and ethanol was added online in order to increase the signal (Wiltsche et al., 2015). The high concentration calibration standard was measured throughout the analysis in order to control for drift in the results. Limits of detection (LOD) and quantification (LOQ) was calculated as 3x and 10x the standard deviation in the control samples respectively.

3.5 *C. elegans* cultivation

The nematodes were maintained on nematode growth medium (51 mM NaCl, 1 mM $CaCl_2$, 1 mM $MgSO_4$, 25 mM KPO_4, 13 µM cholesterol, 17 g/L agar, 2.5 g/L peptone, NGM) plates seeded with *E. coli* OP50 at 20^o C. Culture transfer was performed every two to three weeks in order to keep the culture in good condition and to prevent the influence of dauer pheromone. A 0.5 cm square of NGM with nematodes was transferred to a fresh plate with NGM and OP50, using a sterilized scalpel (Stiernagle, 2006).

Since toxicity tests were performed in liquid media, the nematodes were transferred to Erlenmeyer flasks with liquid culture at least two weeks in advance in order for them to adjust to a different environment. The liquid growth medium consisted of OP50 resuspended in S-base with cholesterol (51 mM NaCl, 1 mM $CaCl_2$, 1 mM $MgSO_4$, 25 mM KPO_4, 0.13 µM cholesterol). The cultures were maintained two times a week by transferring 1 ml of the old nematode culture to a new flask with fresh growth media. The cultures were stored in the dark at 20^o C with gentle shaking (125 rotations/minute) (Stiernagle, 2006).

OP50 was prepared from a – 80^o C glycerol stock, and grown on a streak plate made with lysogeny broth (LB) agar (0.17 M NaCl, 10 g/L Tryptone, 5 g/L yeast extract, and 12 g/L agar) medium. Using a sterilized inoculation loop, the bacteria was streaked across the plate, diluting the liquid culture, and leading to defined colonies formation. The plate was incubated at 37^o C overnight and then kept in a fridge at 4^o C while in use.

The OP50 used in nematode cultivation and in the toxicity tests was prepared a day in advance. Using a sterilized inoculation loop, bacteria were transferred from the LB plate and into an Erlenmeyer flask with liquid LB-medium (0.17 M NaCl, 10 g/L Tryptone and 5 g/L yeast extract). This culture was incubated overnight at 37 °C with shaking at 200 rpm in order to insure sufficient oxygenation. The next day the bacteria were transferred into 50 ml falcon tubes for washing. The tubes were centrifuged at 5000g for 10 minutes, leading to the formation of a bacteria pellet along the wall at the bottom of the tube. The supernatant was removed and an equal volume of S-base (51 mM NaCl) was added. The tubes were then put into the centrifuge for 5 minutes, only rotated 180^{o} so that the pellet would travel to the other side of the tube during centrifugation. This was done twice before the OP50 pellet was resuspended in S-base with cholesterol and transferred into a sterile Erlenmeyer flask.

3.6 Preparation of age synchronized culture

In order to obtain an age synchronized culture of nematodes for an exposure experiment, an alkaline hypochlorite treatment was performed on the nematodes one day in advance. 20 ml of a 3-4 day old culture was extracted and left in a 50 ml falcon tube allowing the nematodes to settle at the bottom. The supernatant was removed and the volume was adjusted back to 20 ml using s-base in order to wash the nematodes. This was repeated twice. Following this, 10 ml of alkaline hypochlorite (7.67 mL ddH_2O, 1.33 mL sodium hypochlorite (425044, Honeywell), 1 mL 5M NaOH) was added and the solution with the nematodes was mixed for 6 minutes using a 5 ml pipette. Bleaching efficiency was controlled by checking the solution for eggs and any unlysed nematodes in a stereomicroscope. Once only eggs remained, the solution was centrifuged at 1000g for 1 minute and the supernatant removed, leaving a pellet on the wall of the tube. The eggs were washed using 20 ml M9 buffer (22 mM KH_2PO_4, 42 mM Na_2HPO_4, 86 mM NaCl, 1 mM $MgSO_4$, pH 6.8) and centrifuged at 1000g for 2 minutes. The supernatant was removed, leaving only the pellet of eggs. This washing was repeated to ensure that the alkaline hypochlorite was removed. The remaining pellet was transferred to a sterile glass beaker. The remaining eggs in the falcon tube was collected in an additional 3 ml of M9, and transferred to the glass beaker. A representative sample was examined using the stereo microscope before the glass beaker was covered with parafilm and stored at 20^{o} C with gentle shaking (125 rpm) incubator overnight. Without any access to food the M9 buffer, the nematodes would be age synchronized at the L1 stage the next day even if the eggs hatched at different times. At this point the nematodes were ready for the toxicity test.

3.7 Standardized toxicity test procedure

The toxicity tests were based on the International Organization for Standardization (ISO) standard for water quality (ISO/TC 147/SC 5, 2010), with some modifications. Due to reasons discussed in chapter 2.1.5, moderately hard reconstituted water (0.44 mM $CaSO_4$, 0.50 mM $MgSO_4$ and 1.14 mM $NaHCO_3$, adjusted with HNO_3 to pH 6.7, MHRW) was used instead of M9 buffer due its low ionic strength. This change is a compromise between optimal conditions for the nematodes, and a stable nanoparticle suspension, but should not have a severe effect on nematode health (Rossbach, 2019)

For the toxicity tests, sterile 24 well culture plates were used (see figure 3.7). Nominal concentrations ranged between 1.56 and 1000 μM for UO_2^{2+}, and 0.78 mg/L and 500 mg/L for UO_2 NPs in triplicate. In order to obtain the desired concentration, the U stock solution was prepared twice as high as the highest exposure concentration. This was in order to compensate for dilution when OP50 was added. 1 ml of U solution was added to the three first wells and 0.5 mL of MHRW was added to the remaining wells. A series of two-fold dilutions were performed by moving 0.5 mL of the U-solution to the next well containing MHRW, mixing with a pipette and repeating for each concentration. After the lowest concentration had been made, excess U-solution was disposed safely, leaving each well with a volume of 0.5 mL. Three wells were left without uranyl and used as unexposed control. *E. coli* was washed as described in chapter 3.4, however, MHRW was used for washing and resuspending the bacteria instead of S-base. For a 2x concentrated *E. coli* suspension, 25 ml of MHRW was added for resuspension. Age synchronized nematodes were examined with the microscope to ensure healthy L1 larvae, and to control the concentration of nematodes. L1s were diluted with M9 if needed. To ensure that there would be a similar number of nematodes in each well (13 ± 5), the beaker containing the nematodes was swirled continuously while adding them. Extra care was taken to avoid cross-contamination of the wells with uranium while using the pipette. The plates were left in the dark at 20^o C with gentle stirring (100 rpm) for 96 or 72 hours for the N2 variant and the GM variants, respectively.

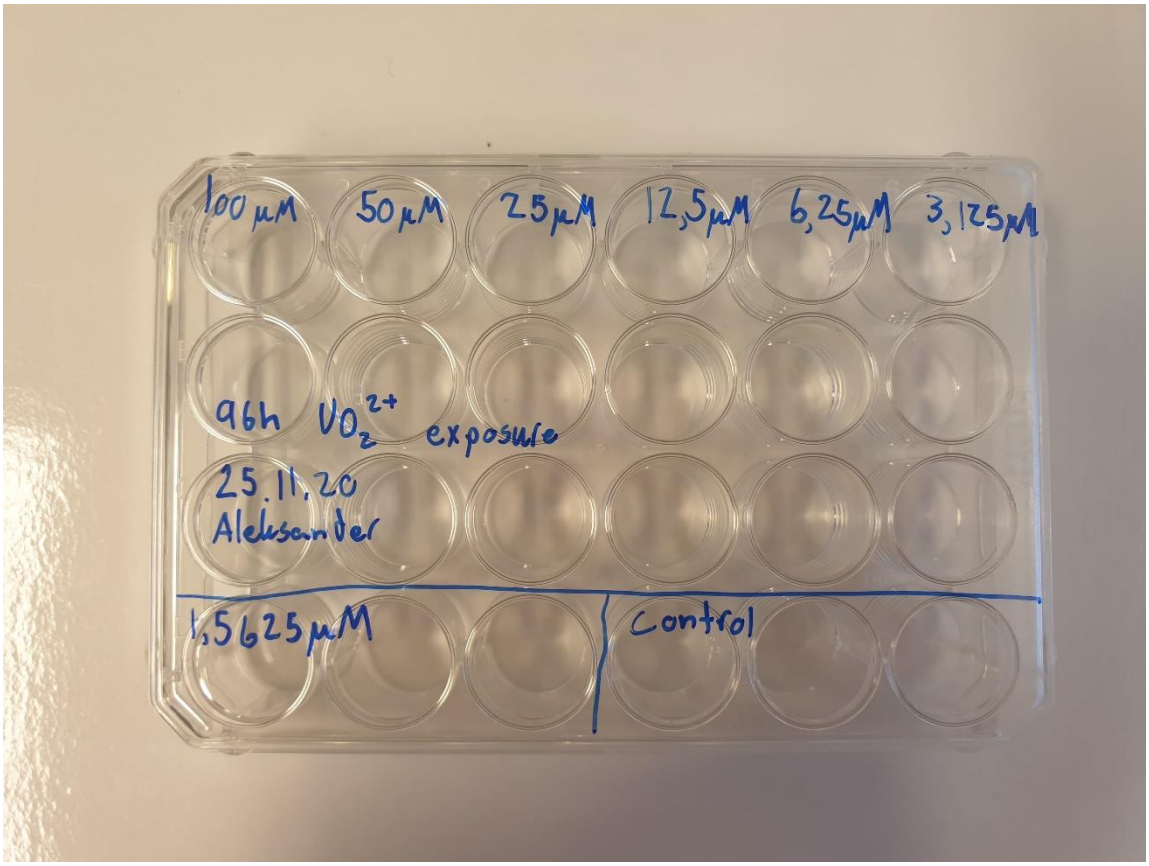

Figure 3.7: Example of the setup of a 24-well culture plate for a 96 hour uranyl exposure. Nominal concentrations ranging from 100 µM to 1.5625 µM, including controls were tested with N2 nematodes in triplicates.

3.8 pH measurements

Using a Multi 340i (WTW) handheld meter with a SenTix 41 (WTW) pH electrode the pH of the MHRW was measured and adjusted to 6.6-6.8 using 0.1 M HNO_3 before preparing the toxicity test. The pH of the exposure media was measured at the beginning and end of the 96 hour exposure period.

3.9 Depuration

Following the 96h exposure, nematodes were extracted from the wells. The pipette-tips used were conditioned in MHRW with 0.2% (v/v) Tween 20 (Sigma-Aldrich) in order to prevent nematodes sticking to the pipette tip walls. The culture plate was tilted and with the help of the pipette the solution in the well was mixed to make sure no nematodes were left in the bottom of the well. The whole content of each well was transferred to separate 15 ml falcon tubes. After letting the nematodes settle at the bottom of the tube, the exposure media was removed, and they were washed twice in 2 mL of MHRW. For the depuration of the nematodes, NGM plates had been prepared by partially covering them with approximately 500 µL OP50 *E. coli*. A 100 µL droplet of the nematodes was placed right next to the *E. coli* lawn and left on the plates for 2 hours. Following this, the plates were checked for tracks to ensure that the nematodes had migrated from the droplet and onto the *E. coli*. In order to collect the nematodes, the NGM plate was tilted and washed with MHRW, avoiding the area where the 100 µL droplet had been applied. In order to make sure that all U measured came from the nematodes, and not the solution itself, a control sample containing no nematodes underwent the same procedure. After counting the remaining nematodes, the samples were moved to clean 15 ml falcon tubes and diluted to 10 ml in 5% (v/v) HNO_3.

For total U uptake in the undepurated nematodes, the same procedure for washing performed, but excluding the depuration step, before diluting them to 10 ml in 5% (w/w) HNO_3. In this manner, the amount of U in the intestines or bound to the outside of the nematode can be differentiated from the amount of U taken up by the nematode. Finally, all samples were incubated at 90^o C for 2 hours to make sure that the nematodes were completely digested by HNO_3.

All samples were then analyzed by ICP-MS as described in chapter 3.4.

3.10 Toxic effect on phenotypic traits

To terminate the toxicity test, 500 µL of 616 µM Rose Bengal was added to each well, and exposure plates were heat treated at 80 °C for 10 minutes. The plates could then be stored in a fridge at 4^o C until assessment of endpoints.

Using a Leica M205 C microscope with a MC 170HD camera, the adult nematodes were studied while remaining in the wells. When visibility was poor, due to Rose Bengal and left over *E. coli*, 0.5 ml of MHRW was added to the well for dilution. After allowing the nematodes time to settle back on the bottom, 0.5 ml was removed from each well. This volume was checked under the microscope to ensure that no nematodes were accidentally removed.

To assess development, the adult nematodes were checked for eggs and total body length using the microscope software (LAS v4.9) to investigate their development. The L1 larvae were counted in each well and divided by the total number of adult nematodes in each well.

To assess visible phenotypic changes, phase contrast images were taken of N2 nematodes *in vivo* following 72h of exposure. Immediately following the exposure period the content from each well was moved to separate Eppendorf-tubes. To ensure no nematodes were left in the bottom of the wells, each well was stirred using the pipette. From the Eppendorf-tubes, a 10 µL droplet containing the nematodes were added to a glass slide. The nematodes were immobilized using 5 µL of a sodium azide solution (1.95 g/L NaN_3) and a glass cover slide was put on top. Images were taken at 10x and 20x magnification using a Leica DM 6B microscope. Approximately 10 nematodes were imaged for each exposure concentration. When the nematodes did not fit inside of one frame, images were stitched to analyze the entire body.

3.11 Fluorescence microscopy of gene modified strains

After 72hs of exposure the SOD-1-, GRX- and HyPer strains of *C. elegans* were imaged *in vivo* using the Leica DM 6B microscope with a Leica DMC 4500 camera. The nematodes in each culture well were transferred to separate Eppendorf tubes. Nematodes were then applied to glass slides and treated with sodium azide (NaN_3) in the same manner as described for the N2 nematodes in the previous chapter.

Nematodes were imaged in fluorescence mode at 10x magnification in order to analyse ROS response. Phase contrast images were also taken to provide a point of reference for the fluorescence images, and to assess the length of the nematodes. If the nematodes were too large to fit inside one image, multiple images were taken. Approximately ten nematodes were imaged this way for each exposure concentration. In the case of SOD-1, where length is needed to normalized intensity, overview images were taken at 2x magnification. SOD-1, reduced GRX, and oxidized HyPer was imaged using a 405 nm excitation and a 535 nm emission filter. Oxidized GRX, and reduced HyPer was imaged using a 490 nm excitation and a 535 mm emission filter. All images were taken in black and white mode.

The images were then analyzed using Leica Application Suite X. The fluorescence was quantified by measuring pixel based average intensity. While different settings were used for different experiments, both for the camera, and the image analysis program, they were always kept consistent within one exposure both for imaging and the analysis. For SOD-1, the intensity was normalized to the total body length of each nematode, which was measured using ImageJ. For GRX and HyPer, the ratio between "oxidized" and "reduced" signal was calculated (Back et al., 2012, Gutscher et al., 2008).

3.12 Statistical analysis

Statistical analysis was performed using R (version 3.4.3). A one-way analysis of variance (ANOVA) was used to check for statistically significant difference between groups. If a difference was identified, a post-hoc Tukey's Honestly Significant Difference (HSD) test was applied to check for significant difference. Differences were considered statistically significant if $p < 0.05$.

Regression analysis was done on the dose-response curves using the build in feature in Microsoft Excel (MSO 365 version). The model was accepted if the coefficient of determination (R^2) was greater than 0.7.

4 Results

4.1 Nanoparticle characterization

Size distribution measurements and zetapotential of the UO_2 NP stock suspension in de-oxygenated ddH_2O was immediately conducted following sonication. The average size from all measurements was 174 ± 8.2 nm (n=5, in triplicates, 10 runs each), while PDI was 0.25 ± 0.033 (n=5, in triplicates, 10 runs each), meaning there was some degree of polydispersity in the suspension. Measurement of electrophoric mobility showed a zeta potential of -9.9 ± 0.19 mV (n=2) indicating that the NPs had a negatively charged surface.

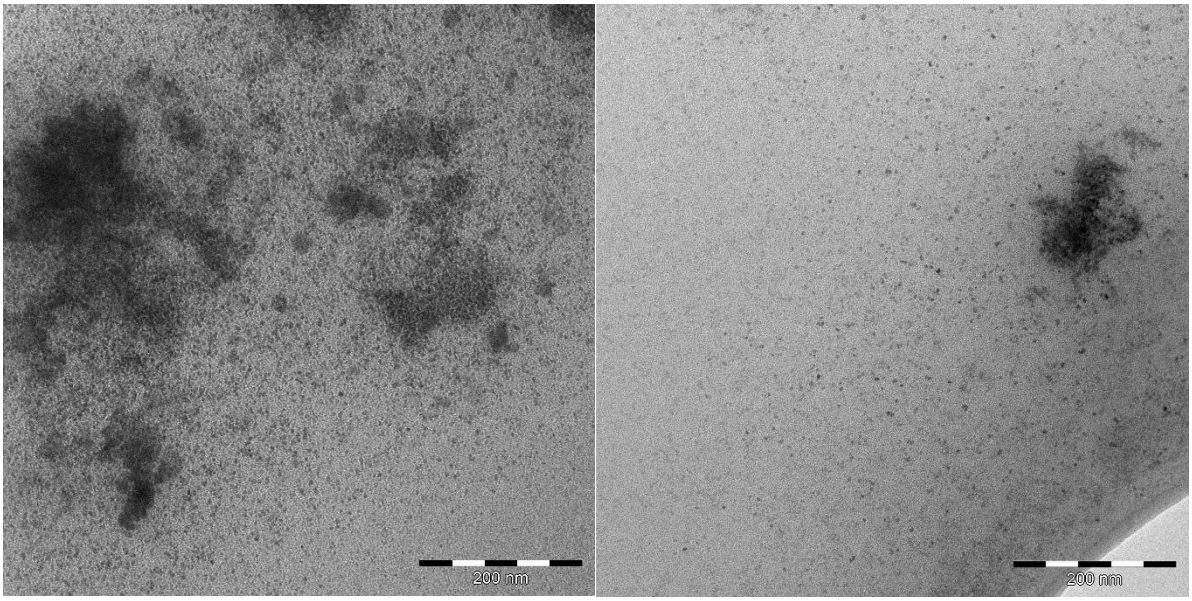

Figure 4.1: TEM images of UO_2 NP suspension on a perforated carbon copper grid. Several images were taken of different areas to obtain a representative number of samples for size measurement. Images were taken at 80 keV, and a 200 nm scalebar is given in each image.

The NP suspension was imaged using TEM and the resulting micrographs showed a mixture of suspended nanoparticles and large agglomerates (figure 4.1). Measuring the agglomerates would yield an artificially high particle size. For this reason, areas in the image without agglomerates were manually chosen and analyzed using ImageJ and the measured average NP diameter was 5 ± 1.4 nm (n=334).

4.2 Exposure conditions

Stocks of both UO_2^{2+} and UO_2 NPs were prepared for use in exposure studies, and concentrations were monitored using ICP-MS analysis (See table 4.2.1 and 4.2.2). While U-concentration that was determined during ICP-MS analysis, this is equivalent of UO_2^{2+} and UO_2 concentrations. For this reason, UO_2 NP concentration is reported as molarity of UO_2. The suspensions used for the standardized toxicity test and the phase-contrast imaging were not measured due to a miscommunication and concentration had to be estimated from the other suspensions. The concentration in the different stocks varied quite substantially giving the estimate a high standard deviation, meaning the concentration in the last two stocks could not be determined accurately.

Table 4.2.1: UO_2 NP concentration in the nanoparticle suspensions prepared for each experiment. Note that the UO_2 NP concentration the stocks used for the toxicity test and imaging are estimated (mean ± standard deviation [SD]) from the other stock concentration.

Associated experiment	**UO_2 NP stock concentration (µM)**
GRX exposure & uptake	2340
HyPer exposure	2140
SOD-1 exposure	3030
Size fractionation	2570
Toxicity test & imaging	2500 ± 380

Uranium concentrations in each triplicate of exposure wells were determined using ICP-MS and compared to the concentrations estimated from the stock concentration (See table 4.2.2). In most cases the measured concentration was lower than the estimated concentration. The ICP-MS measurement of UO_2 NP stocks were used to calculate concentrations for each dilution in exposure studies. Total U concentrations were measured from selected exposure concentrations (low, medium and high) were measured at start and end of each exposure (See table 4.2.2). The uranyl concentration for the remaining wells were imputed based on the mean of measured recoveries.

Table 4.2.2: U concentrations (mean ± SD, n=3) estimated from stock dilution and measured concentration at the beginning (T-0h) and end (96h) of the exposure period. Recovery was calculated at T-0h from the estimate, and at 96h from T-0h.

Species	**Estimated concentration (µM)**	**Measured concentration at T-0h (µM)**	**Recovery (%)**	**Measured concentration at 96h (µM)**	**Recovery from T-0h (%)**
UO_2^{2+}	6.25	4.8 ± 0.52	77	4.4 ± 0.29	91
	25	24 ± 1.6	95	27 ± 1.8	114
	100	102 ± 3.8	102	116 ± 6.6	114
UO_2 NP	20.1	18 ± 1.1	88	19 ± 1.7	110
	40.1	38 ± 2.9	94	40.0 ± 0.54	106
	80.3	71.0 ± 0.67	89	74 ± 1.8	104
	161	143 ± 6.0	89	145 ± 7.8	102
	321	250 ± 15	77	294 ± 5.7	119
	642	460 ± 35	72	560 ± 15	120
	1280	1160 ± 32	91	1200 ± 239	102

The pH in the exposure media was measured at the beginning and end of the 96 hour exposure period. At the beginning of the exposure, pH was measured at 7.1 ± 0.11. At the end of the exposures pH in the exposure media had increased further to 7.42 ± 0.05.

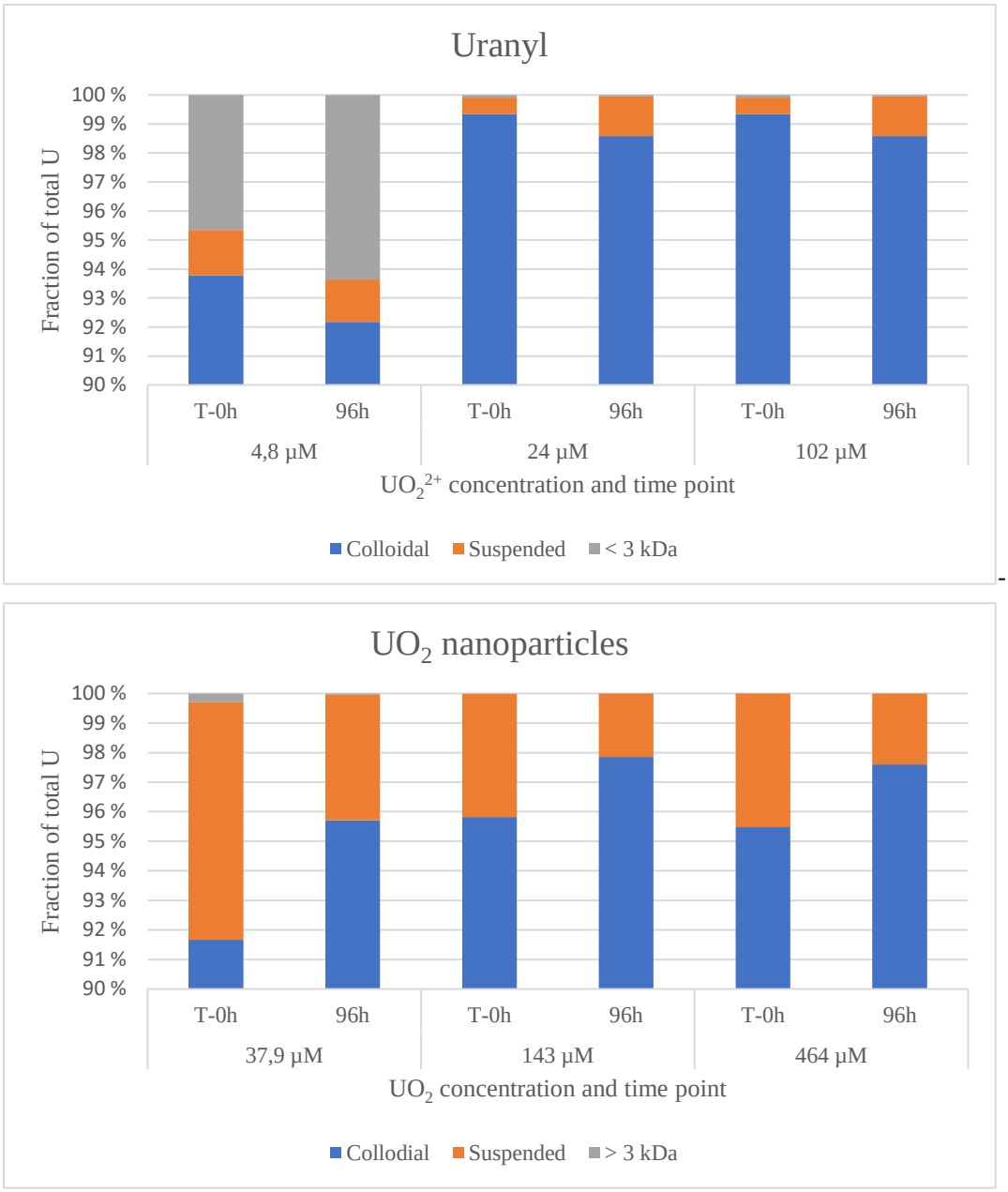

Figure 4.2: Size fractionation of U in uranyl (top) and UO_2 NP (bottom) exposure. Three exposure concentrations were analyzed at T-0h and 96h. The data represent an average of triplicate measurements. Note that the Y-axis starts out at 90%, the remaining 90% belonging to the colloidal fraction.

The fractionation analysis showed that U was found largely in the colloidal size fraction both for ions and NPs, while less than 0.3% U was found in the > 3kDa fraction, with the exception of the 4.8 µM UO_2^{2+} exposure. Additionally, the suspended fraction in the UO_2 NP exposure was substantially higher than in the UO_2^{2+} exposure. For the ions a slight decrease of UO_2^{2+} in the colloidal fraction after the 96 was observed. Meanwhile, in the nanoparticle suspension the colloidal fraction of UO_2 NP increased.

4.3 Standard toxicity test

The toxicity of both UO_2^{2+}, and UO_2 NPs were assessed by performing 96 hour exposure studies using a wide range of concentrations (table 4.2.2). In these studies the lowest concentrations which yielded a 100% mortality were 277 µM UO_2^{2+} and 1100 ± 173 µM UO_2 NP. For lower concentrations the dose-response of the two species were assessed using several different toxicological endpoints (see figure 4.3.1).

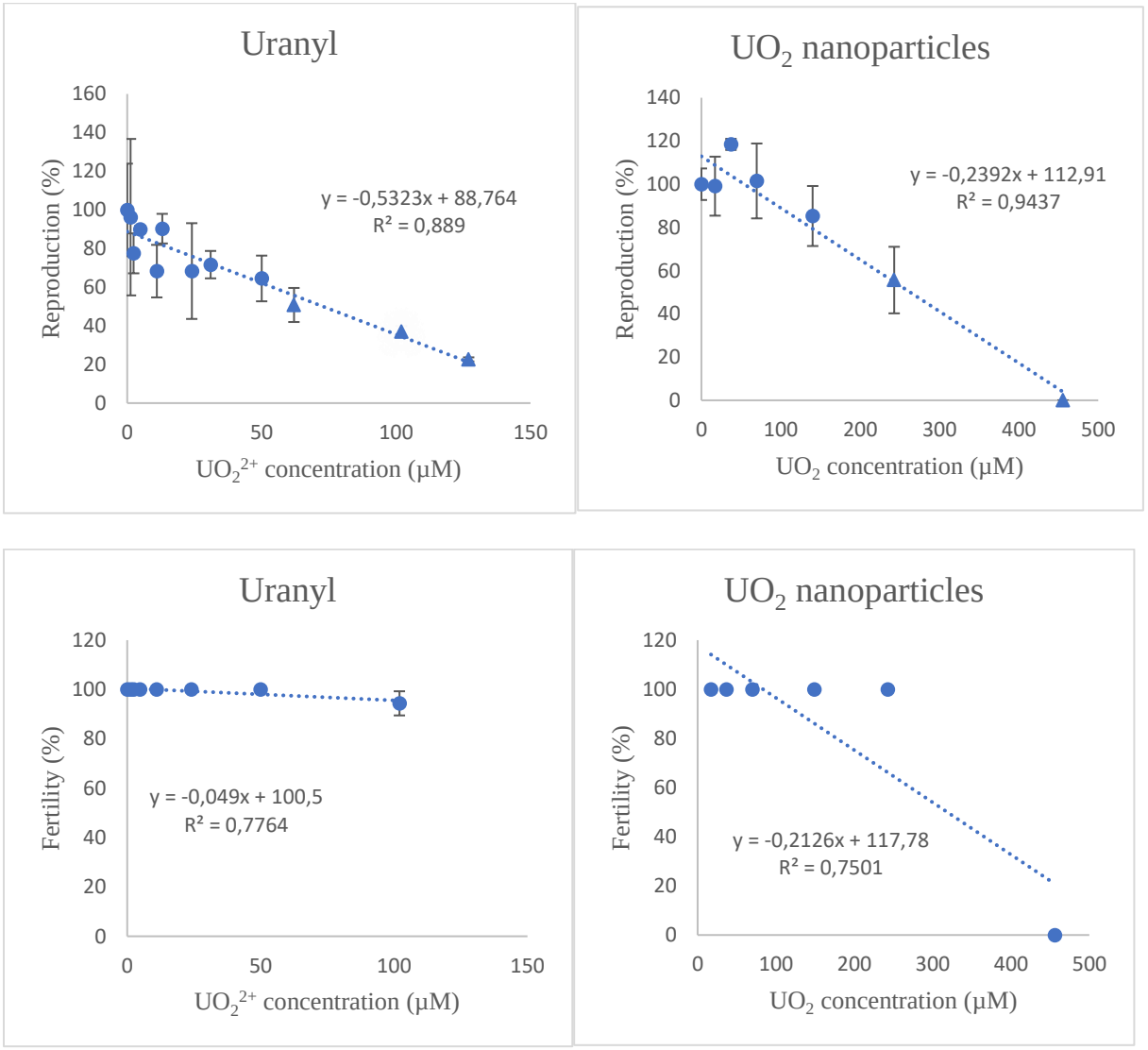

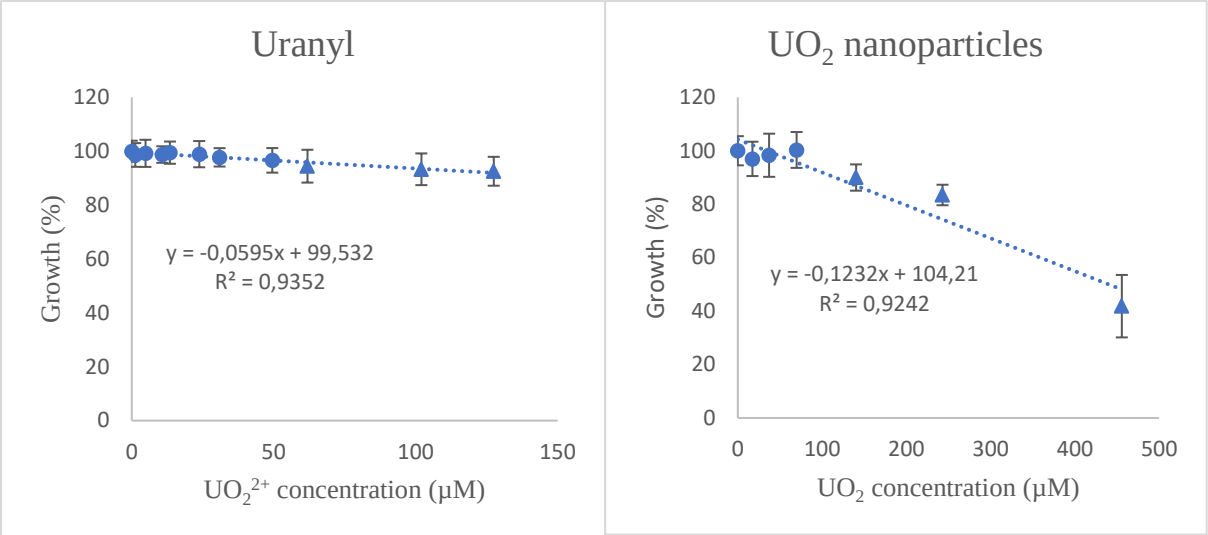

Figure 4.3.1: Dose response for reproduction, fertility and growth in *C. elegans* exposed to different concentrations of U in the form of ions and nanoparticles. Data points which were significantly different to their respective control ($p < 0.05$, Tukey's HSD) are marked as triangles.

In the UO_2^{2+} exposure a statistically significant decrease in both reproduction ($p=0.007$, Tukey's HSD) and growth ($p=0.0002$, Tukey's HSD) at 62 µM UO_2^{2+} was observed, although the reduction in growth was very slight. No significant reduction in fertility was measured. In the nanoparticle exposure a significant decrease in growth was observed at 140 ± 21 µM UO_2 NP ($p=2\times10^{-16}$) and a significant decrease in reproduction at 240 ± 27 µM UO_2 NP ($p=0.006$). At 460 ± 69 µM UO_2 NP fertility was reduced to 0% with no reproduction.

Linear regression showed a correlation between dose and response in all endpoints for both UO_2^{2+} and UO_2 NP (Figure 4.3.1). The slope number of the linear regression model for reproduction in the UO_2^{2+} exposure was twice of that in the UO_2 NP exposure. For fertility and growth the value was greater in the UO_2 NP exposure.

Half maximal effective concentration (EC_{50}) and 10% effect concentration (EC_{10}) was calculated for reproduction using the web-interface MOSAIC (Charles et al., 2018) and are given in table 4.3. Both EC_{50} and EC_{10} values were substantially higher for UO_2 NPs than the UO_2^{2+}.

Table 4.3: EC_{10} and EC_{50} values for reproduction in nematodes exposed to UO_2^{2+} and UO_2 NPs.

	EC_{10} [95% confidence interval](μM)	**EC_{50} [95% confidence interval] (μM)**
UO_2^{2+}	7.36 [1.36 - 22.1]	56.3 [147 – 237]
UO_2 NPs	209 [34.1 – 81.7]	244 [225 – 268]

Phase contrast images were taken of nematodes exposed to UO_2^{2+} and UO_2 NPs after a 72 hour exposure period (see figure 4.3.2 and 4.3.3). The images taken of nematodes exposed to UO_2^{2+} showed little difference in nematodes. Some nematodes had fewer oocytes, and a few individuals showed malformations. Unexpectedly this seemed to be more frequent in the 50 μM group than the 102 μM group.

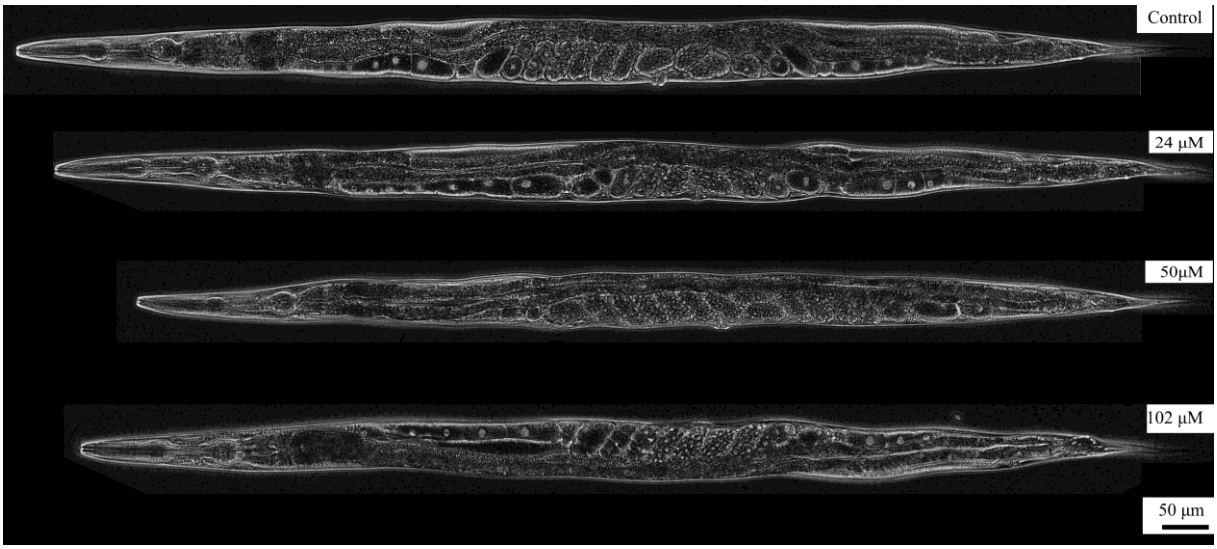

Figure 4.3.2: Representative examples of phase contrast images taken of nematodes after a 72 hour uranyl exposure.

Images taken of nematodes exposed to UO_2 NPs showed a couple of notable physiological differences between the control group of nematodes and the higher exposure groups. Nematodes exposed to 243 μM and 456 μM UO_2 NP were not pregnant, and were shorter than the controls. Additionally, these nematodes had a disproportionately large pharynx compared to overall body length. This was investigated further by measuring the length of the pharynx (from the tip of the snout to the back of the grinder, see figure 4.3.4) and the difference was statistically significant (see figure 4.3.5).

Additionally, the lumen of the intestines appeared to be much wider in the high concentration groups compared to the control group. The width of the lumen and the body (right in front of the gonad, see figure 4.4.4) was measured, and statistical analysis confirmed that the lumen was significantly wider compared to body width in higher concentrations (figure 4.3.5). The intestines of nematodes in the 456 µM UO_2 NP exposure group also looked contorted in several individuals.

Images taken of nematodes exposed to U ions were assessed to check for changes in pharynx-to-body length ratio and lumen-to-body width ratio. However, no significant difference could be found between the control group and the highest concentration (p=0.194 and p=0.393 respectively) and it was not investigated further.

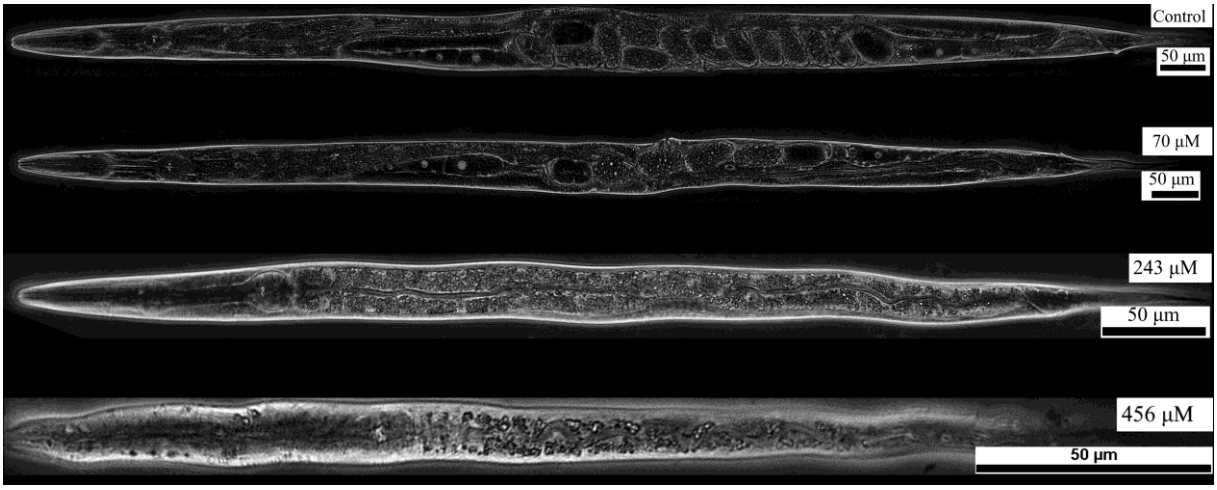

Figure 4.3.3: Representative examples of phase contrast images taken of nematodes after a 72 hour uranium nanoparticle exposure. Note that the scalebar varies between each image.

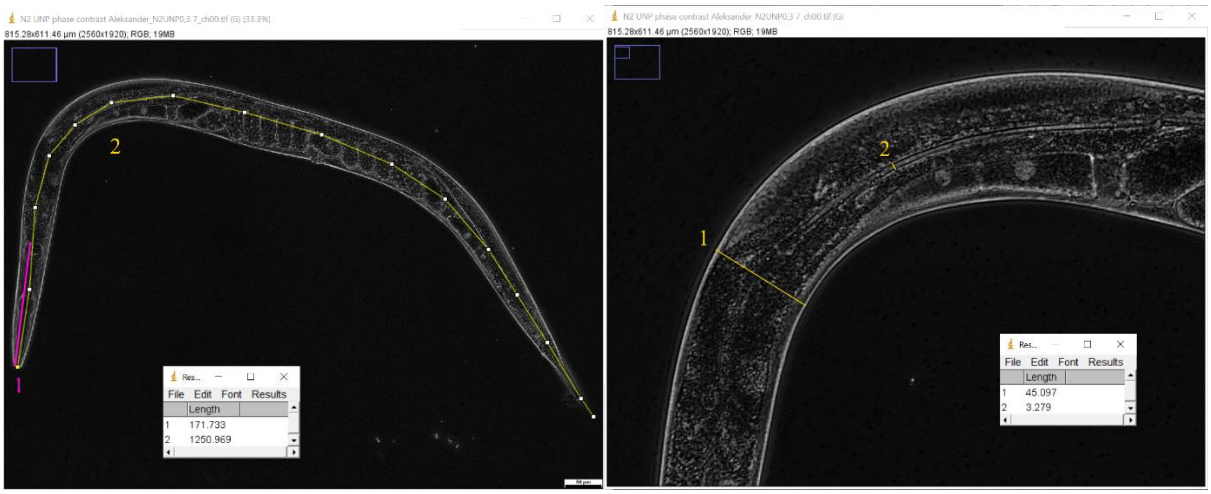

Figure 4.3.4: Measurement of pharynx and body length (left), and lumen and body width (right) in ImageJ.

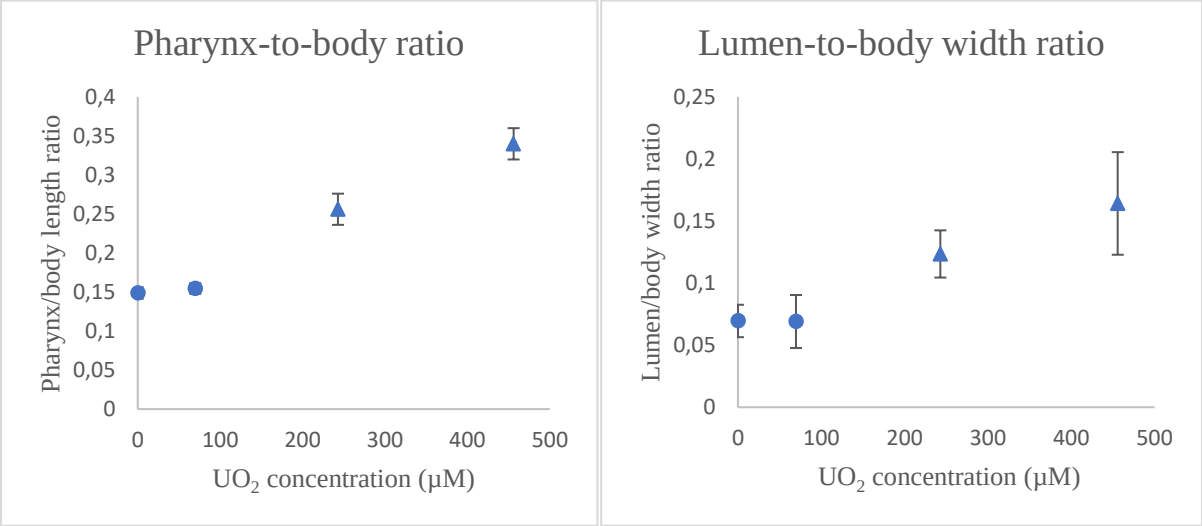

Figure 4.3.5: Change in pharynx-to-body length ratio and lumen-to-body width ratio as an effect of UO_2 NP concentration in the 72h nanoparticle exposure. Groups that are significantly different from the control group are marked as triangles

4.4 Uranium uptake

Uranium concentrations were measured in nematodes, both before and after depuration following 96 hours of exposure, by ICP-MS (table 4.4). A control set of without nematodes was also measured with the UO_2^{2+} exposure in order to ensure that no exposure media was included after depuration. These samples were all below the the LOD of the depurated nematodes, with the exception of the 102 µM exposure group, which was under the limit of quantification (LOQ, $10xSD_{Control}$).

In general a higher exposure concentration resulted in a higher concentration of U in the nematodes, with the exception of the 131 µM UO_2 NP exposure. Here, the UO_2 NP concentration in the depurated nematodes were below the LOD. The U concentration in the undepurated nematodes were at least 4 times higher than the concentration in the depurated ones.

Table 4.4: U concentrations (mean ± SD) measured in nematodes exposed to different concentrations of U ions and nanoparticles. The LODs were 1: 0.00018 pmol, 2: 0.0018, 3: 0.00076 pmol, and 4: 0.0073 pmol U.

U Species	**Exposure concentration (µM U)**	**Undepurated (pmol U per nematode)**	**Depurated (pmol U per nematode)**
UO_2^{2+}	0	<LOD[1]	<LOD[2]
	4.8	0.08 ± 0.014	0.02 ± 0.012
	24	0.40 ± 0.042	0.03 ± 0.011
	102	1.3 ± 0.15	0.09 ± 0.04
UO_2 NP	0	<LOD[3]	<LOD[4]
	34.7	7 ± 2.9	0.09 ± 0.077
	131	3.5 ± 0.75	<LOD[4]
	425	110 ± 17	5 ± 6.8

In order to assess the correlation between uptake and toxic effect, uptake was plotted against the response in the corresponding exposure concentration (see figure 4.4.1 and 4.4.2). This was done for reproduction and growth, since these endpoints had the best dose-response correlation, in both undepurated and depurated nematodes. Regression analysis showed much greater slope number in dose-response in both the undepurated and depurated nematodes from the uranyl exposure than in the UO_2 nanoparticle exposure.

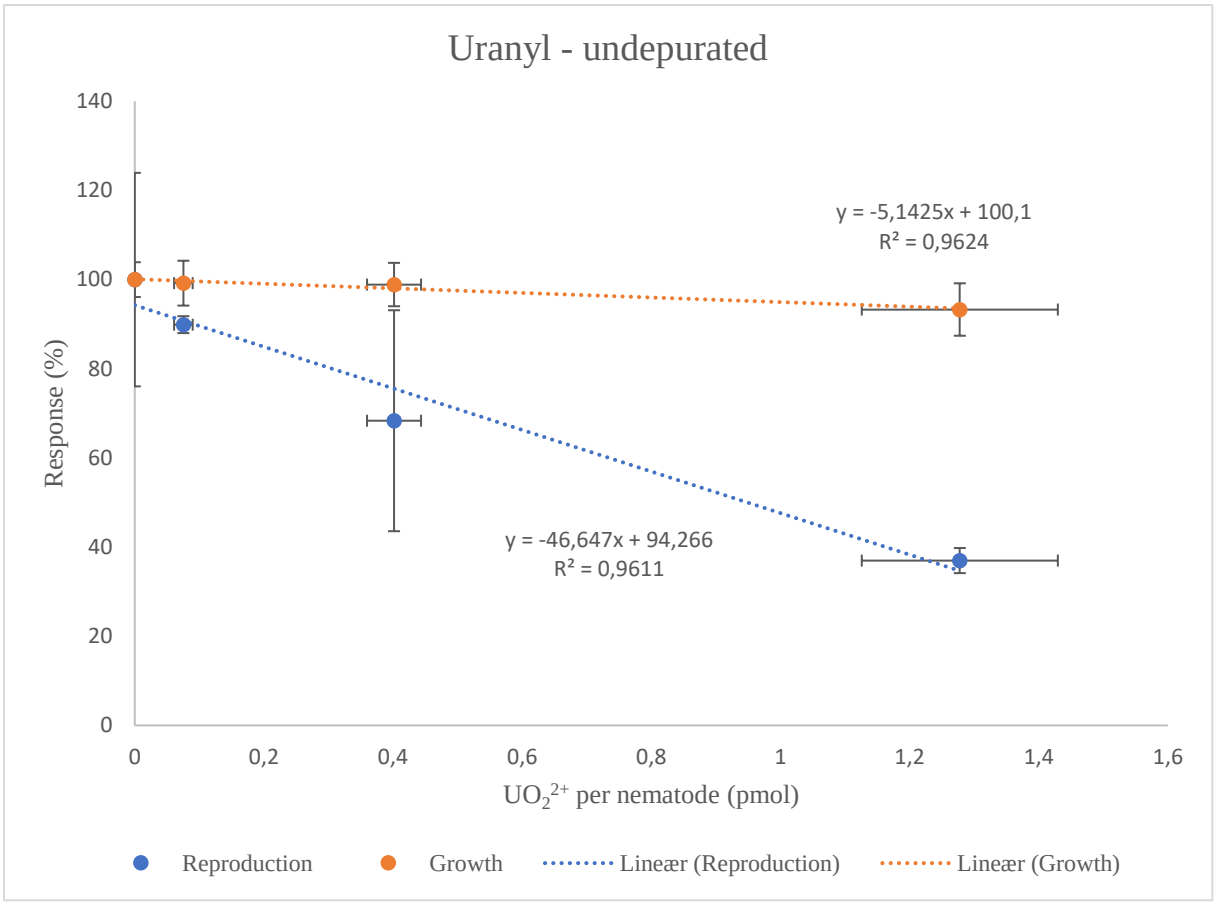

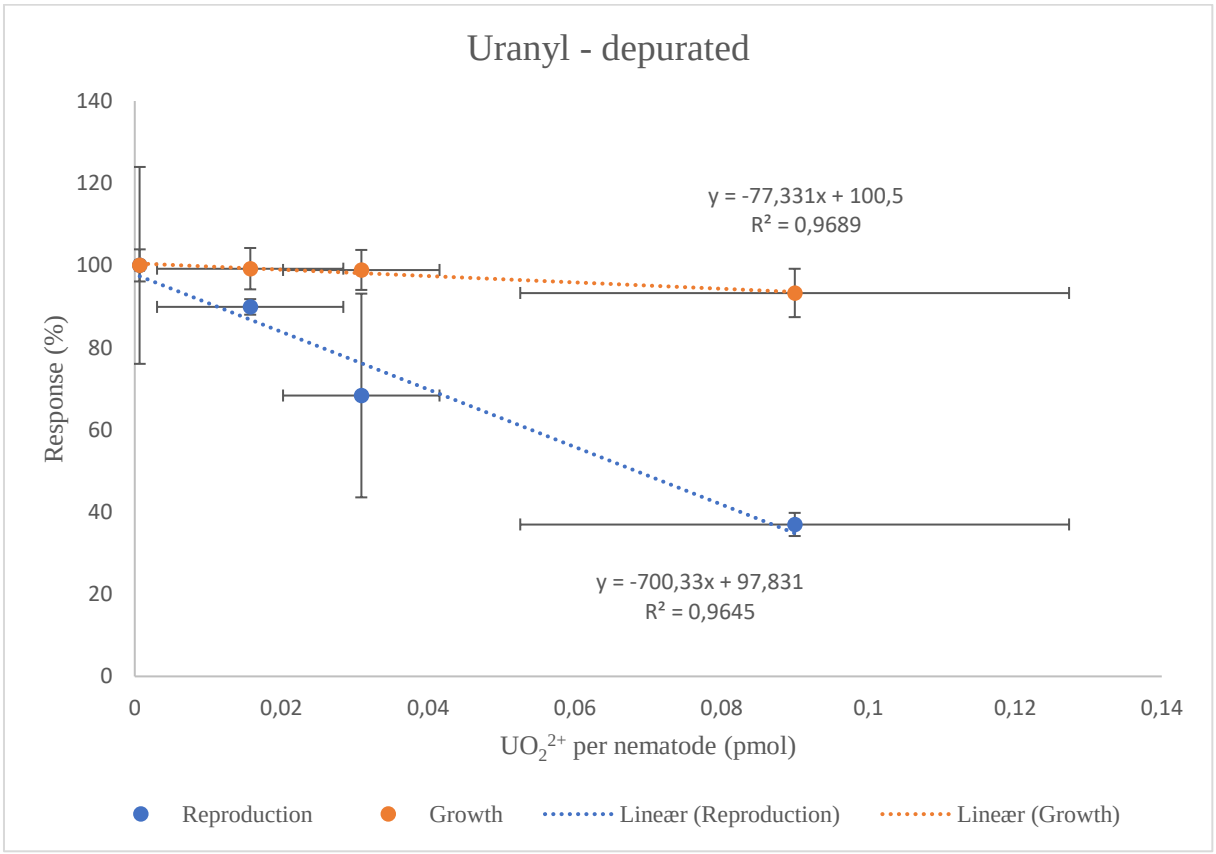

Figure 4.4.1: Uptake of UO_2^{2+} and response in reproduction and growth. Regression lines with formula and R^2-values are also included.

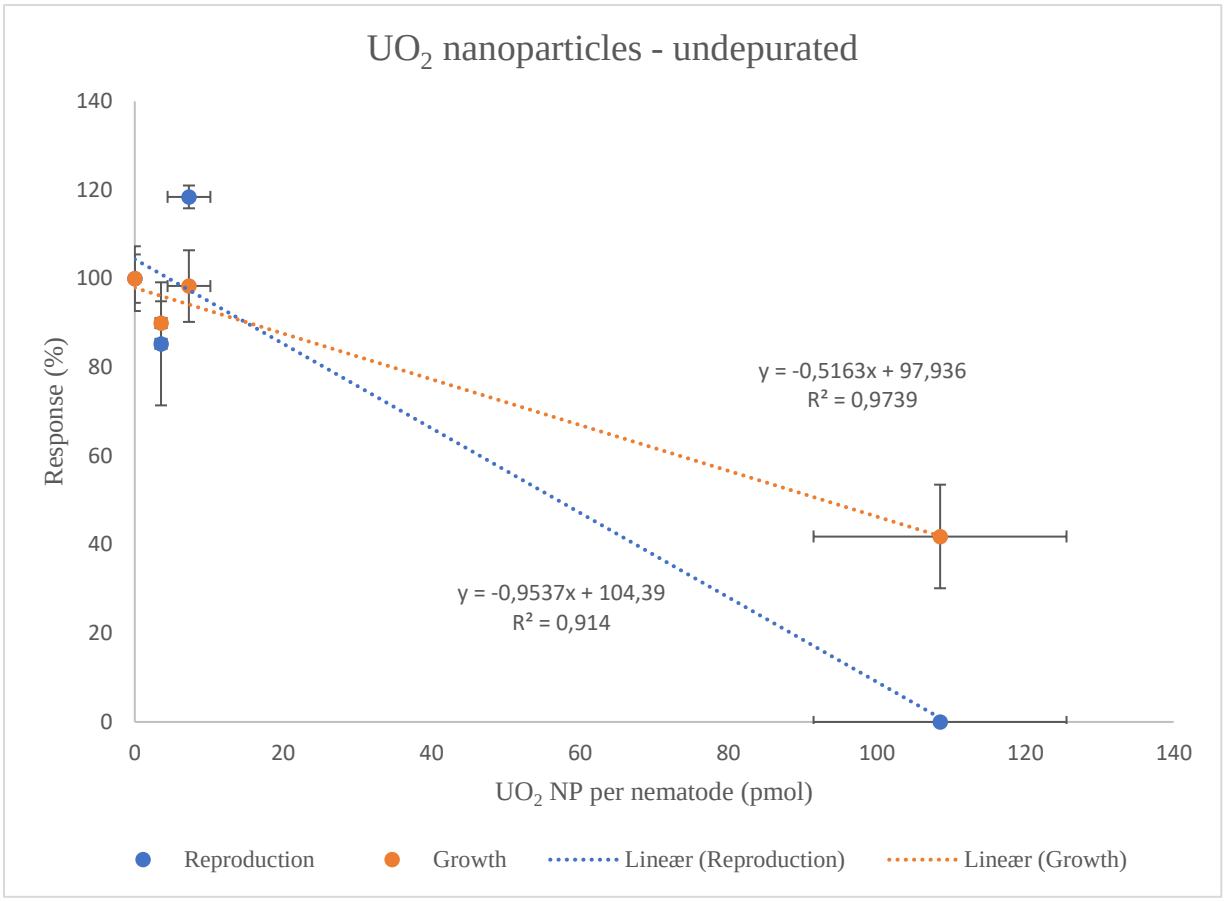

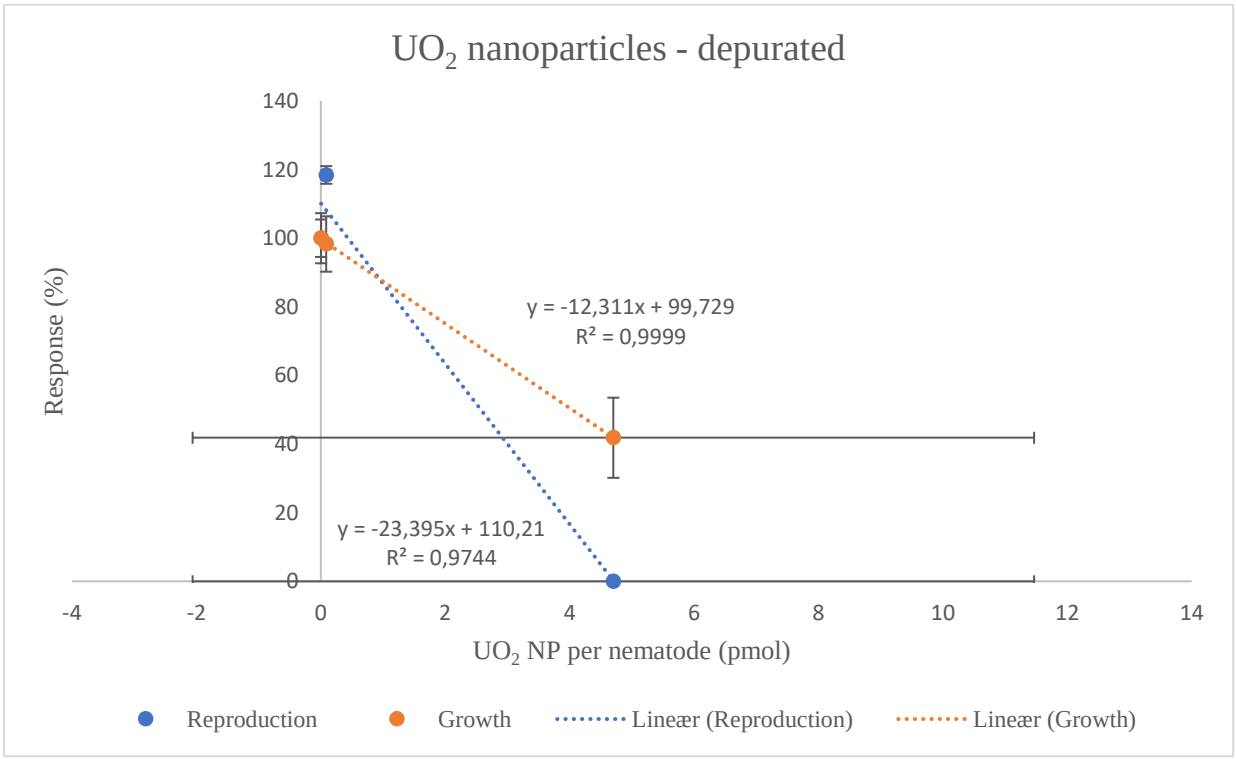

Figure 4.4.2: Uptake of UO_2 NPs and response in reproduction and growth. Regression lines with formula and R^2-values are also included.

4.5 Oxidative stress response

Oxidative stress response in *C. elegans* was assessed using fluorescence microscopy to image three different GM-strains: SOD-1, HyPer, and GRX. However some technical challenges were encountered with the HyPer and GRX strains and the results from these analyses are included in the appendix.

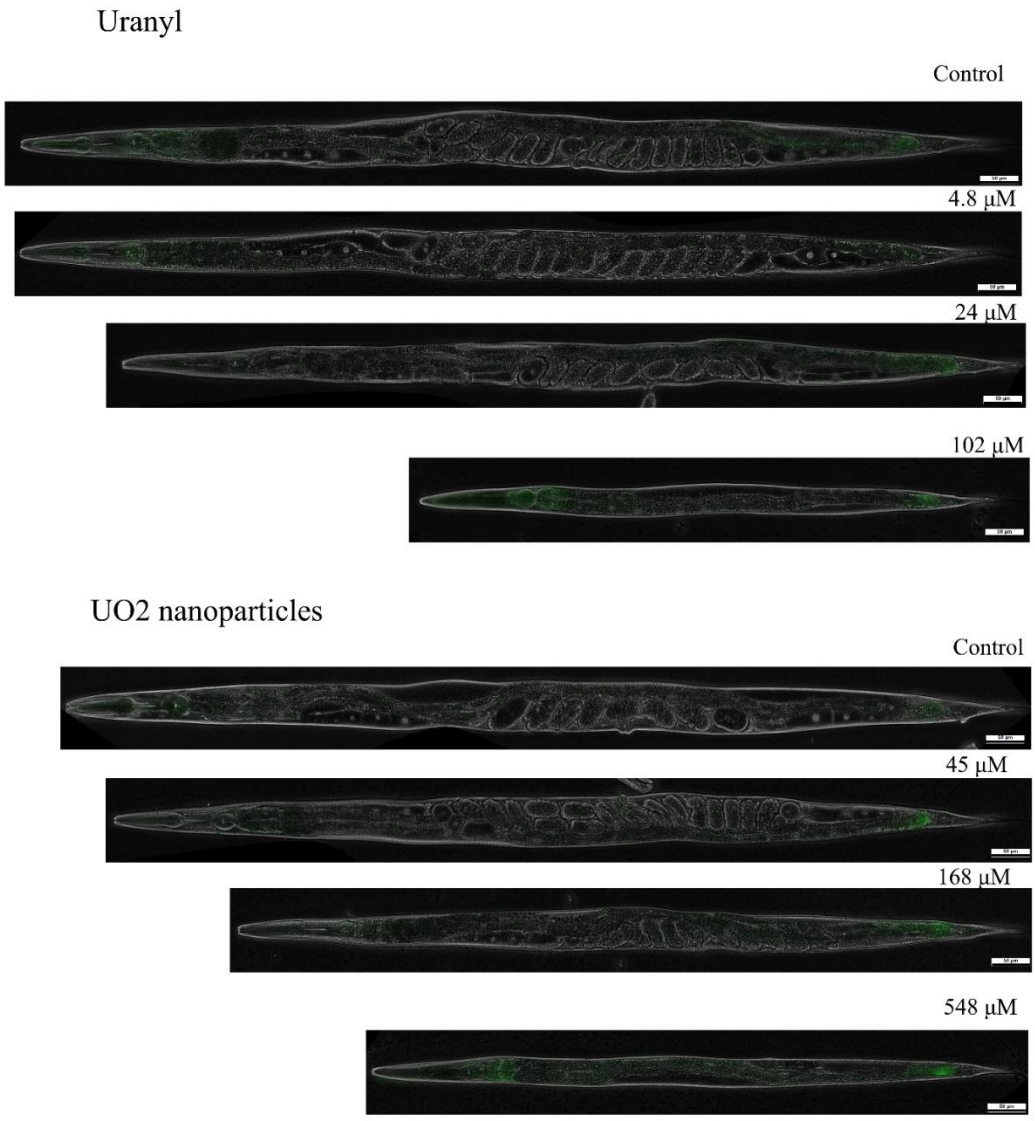

Figure 4.5.1: Representative examples of phase contrast images with fluorescence overlay taken of SOD-1 strain nematodes exposed to uranyl and UO_2 nanoparticles at 72h. Nematodes were straightened using ImageJ and 50 µm scalebars are included in each micrograph.

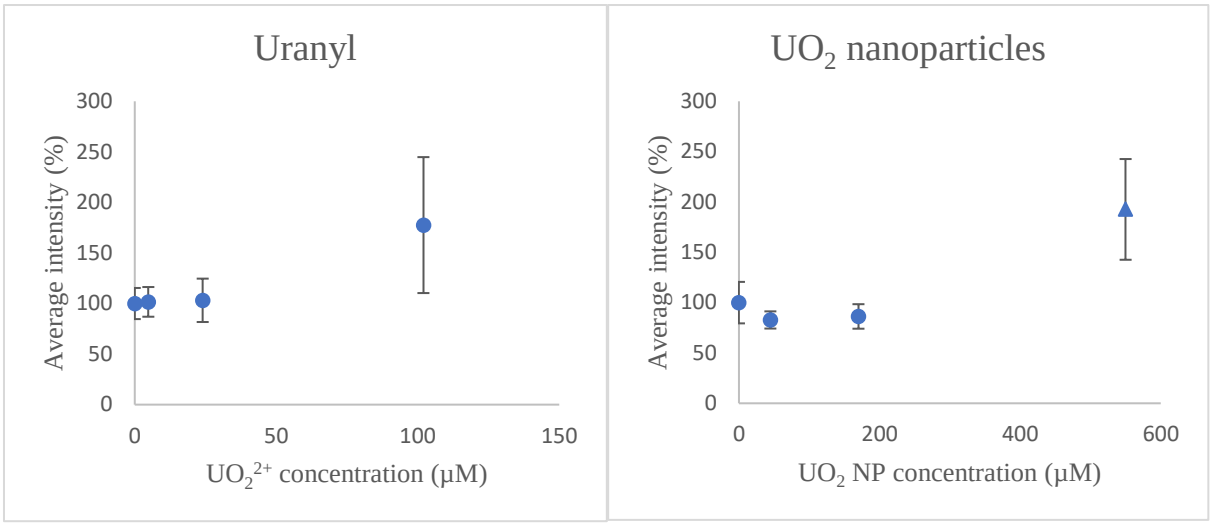

Figure 4.5.2: Measured intensity in SOD-1 nematodes exposed to different concentrations of U in the form of ions and nanoparticles. Data points that were significantly different to their respective control are marked as a triangle.

Image analysis of SOD-1 revealed no significant difference between exposure groups could be identified from nematodes in the ion exposure (Figure 4.5.2). There was a slight, but not significant ($p= 0.1947$), increase in average intensity at 102 µM UO_2^{2+}. In the NP exposure there was a statistically significant ($p=5\times10^{-6}$) increase in average intensity at 548 µM UO_2 NP indicating an increase in SOD-1 expression (Figure 4.5.2).

5 Discussion

5.1 Nanoparticle characterization

Nanoparticle size in the UO_2 NP suspension was characterized using several different methods. Firstly, DLS measurements of the nanoparticle suspension showed an average hydrodynamic particle diameter of 174 ± 8.2 nm. This is several times larger than the 3 to 15 nm specified for the dry particles after production (Pavelková et al., 2013) and is likely caused by large agglomerates dominating the signal (i.e. light scattering). The PDI was 0.25 ± 0.033, which is higher than what is expected for a monomodal size distribution (Malvern Instruments, 2013). Furthermore, TEM analysis revealed that the NP suspension was a mixture of large agglomerates and individual NPs. Therefore, the high PDI combined with the TEM observations of presence of larger aggregates could explain the high size distribution measurements from the DLS. Nevertheless, through image analysis of the TEM micrographs, the diameter of these particles were revealed to be around 5 nm which is more in line with what was expected and specified by the supplier.

In addition to the high PDI which is an indication of low stability of the particle suspension, the zeta potential of the nanoparticles was measured at -9.9 ± 0.19 mV. The slight negative charge suggests a limited electrostatic repulsion between particles, even with the NM-300KDIS Ag-dispersant coating. In turn, this may result in a relatively poor suspension stability, which could explain the aggregation observed with TEM (Kumar and Dixit, 2017).

5.2 Exposure conditions

Total U concentrations measurement in the exposure media showed a slight increase in concentration from the start (T-0h) to the end (96h) exposure (see table 4.2.2). A possible cause for this could be the liquid of the exposure wells evaporating leading to a higher U concentration. Depending on when this happened, this could mean that the nematodes were exposed to a higher concentration than planned. However, in most cases, this change was very slight (<10%) and would likely not affect the response.

As mentioned in chapter 4.2 the U concentration of two of the NP suspensions were not measured as the sonication was expected to yield a more consistent suspension. For this reason, the UO_2 NP concentration in suspensions used for the standardized toxicity test, and imaging had to be estimated from the remaining suspensions. This estimation had a quite high relative standard deviation of 15 %. While this does not affect the uncertainty in toxic response, it does increase the uncertainty of the effect concentration assessment (table 4.3.1).

The pH measurements of the exposure media at the beginning and end of a 96 hour exposure period showed that pH increased from 7.1 to 7.42. This change could have influenced the uranyl speciation, leading to a higher amount of $UO_2(CO_3)_2^{2-}$ (see figure 2.1) As described in chapter 2.1, while negatively charged uranyl-species have a high mobility in water, they have poor interactions with the cell membrane leading to reduced bioavailability and toxicity, as has been shown by several studies (Zeman et al., 2008, Hyne et al., 1992).

The size fractionation experiment revealed that a large majority of the U in the ion exposure media were found in the colloidal fraction, while U in the < 3 kDa fraction, which is usually associated with low molecular mass (e.g. ions), was less than 0.1% in most cases. A likely explanation for this is that since the *E. coli* cells have a negatively charged surface, uranyl ions may interact with the bacterial cell surface and become absorbed by the bacteria (Dickson and Koohmaraie, 1989, Kulkarni et al., 2016). Thus, leading to uranyl exposure when ingested by the nematodes (Goussen et al., 2013).

Likewise, in the NP exposure media the UO_2 NP was found mostly in the colloidal fraction, with a comparatively small fraction of suspended U, which was attributed to individual UO_2 NPs. Since Zeta potential measurements of the nanoparticles showed that the NPs were slightly negatively charged, it is unlikely that they are bound to *E. coli* in the same way as the ions. If the colloidal fraction was mostly ions dissociated from the NPs, there should have been a much greater response in toxicological endpoints, considering the response in the ion exposure. For this reason the colloidal fraction is likely comprised largely of NP agglomerates and only a small amount of ions . These agglomerates may enable faster uptake rates by oral ingestion, but may also be less bioavailable than individual NPs due to a larger size (Ellegaard-Jensen et al., 2012, Ma et al., 2009).

5.3 Toxic effects of UO_2 nanoparticles compared to uranyl

Chronic toxicity tests with UO_2^{2+} ions and UO_2 NPs were performed, and reproduction, fertility and growth in the N2-strain of *C. elegans* were assessed. While UO_2^{2+} and UO_2 NPs were made from DU and natural U respectively, toxic responses reported in this work was assumed to be caused by chemical toxicity.

The upper concentration limit in the exposures was defined by a 100% mortality. In the ion and NP exposures these concentrations were 255 µM UO_2^{2+} and 1100 µM UO_2 NPs respectively. To put this in perspective: from samples taken of groundwater mostly around the Oslofjord and Bergen areas in Norway concentrations up to 3.2 µM U were measured (Frengstad et al., 2000). In groundwater from the Helsinki region of Finland the highest concentration measured was 58.82 µM U, which was considered anomalously high (Asikainen and Kahlos, 1979). Thus, the lethal concentrations reported in the present study are far greater than what could be considered environmentally relevant.

On the other hand, previous U exposure studies conducted with *C. elegans* have used higher U concentrations than what was tested in the present work. Nematodes are reported to survive while being exposed to >1 mM UO_2^{2+} (Dutilleul et al., 2013, Jiang et al., 2009) with no observed effect on reproduction in one case (Lu et al., 2020). However, these exposure studies were conducted using NGM plates instead of the MHRW liquid exposure media used in the present work. The difference in dose-response might therefore be due to the difference in ionic strength, presence of complexing anions, or possibly pH reducing the bioavailability of the uranyl (Tyne et al., 2013, Fortin et al., 2004, Choppin, 2007).

The two-fold dilution series applied in the present work resulted in larger gaps between exposure groups, leading to possible uncertainties about exact lethal concentrations (Table 4.2.2). This means that 100 % mortality might occur at lower concentrations. Another consequence from this is that the full range of some responses remain undiscovered, as tests using just below lethal concentration were not necessarily conducted.

The least sensitive endpoint was fertility (Figure 4.3.1). No significant reduction in fertility was observed, except for in the highest concentration group of the NP exposures. This could suggest a mere delay of the development and reproduction. This has been reported in another study, where differing cumulated number eggs in different exposure concentrations converged over time (Goussen et al., 2015).

In the nematodes exposed to 140 μM UO_2 NPs, growth was reduced to 90% compared to that of the control at and further to 40% at 460 μM UO_2 NPs (Figure 4.3.1). Comparatively, in the ion exposure, growth was reduced to 93% compared to the control at 128 μM UO_2^{2+}. The data showed that UO_2^{2+} and UO_2 have quite similar effect on growth in *C. elegans*. However , considering the effects on reproduction and the high concentration of UO_2 NPs required to elicit a substantial reduction in growth, it is likely that the growth reduction in the ion exposure would have been greater closer to 255 μM UO_2^{2+}.

The most sensitive endpoint was reproduction with a significant reduction in both the ion and NP exposure (Figure 4.3.1). In the NP exposure reproduction was reduced to 60% compared to the control group at 240 μM UO_2 NPs. In the UO_2^{2+} exposure reproduction was reduced to 51% at 62 μM. Furthermore both EC_{10} and EC_{50} values were much higher for UO_2 NPs than UO_2^{2+} (Table 4.3). The UO_2 NP concentration required induce a 10% effect was 28 times greater then the UO_2^{2+} concentration. In order to induce a 50% effect the concentration of UO_2 NP was four-fold that of UO_2^{2+}. Thus, UO_2^{2+} has a much greater effect on reproduction than UO_2 NPs.

Regression analysis of the toxicity test results (Figure 4.3.1) revealed two-fold steeper response in reproduction in the UO_2^{2+} exposures than in the UO_2 NPs exposures further indicating that the uranyl is more toxic to the nematodes than the nanoparticles. However, from the other regression analysis, fertility and growth seems to be less sensitive to UO_2^{2+} than UO_2 NPs. This is likely due to the poor resolution of data-points at the highest exposure concentrations as no substantial effects were observed in either growth or fertility in the UO_2^{2+} exposure.

Phase contrast images were taken of nematodes in order to determine whether the toxic response could be related to developmental defects or phenotypical abnormalities. Images taken from the NP exposure showed a disproportionately large pharynx in nematodes exposed to high concentrations of NPs (Figure 4.3.3). The development of the pharynx in *C. elegans* is robust, even with abnormal development in other tissues, due to conserved molecular pathways utilizing multiple sets of transcription factors (Mango, 2007, Mörck et al., 2003). In this case, it could mean that the development of the pharynx is less affected by the uranium than the rest of the nematode, thus leading to the pharynx growing disproportionately big compared to the rest of the body.

Simultaneously, the lumen of the intestine was significantly wider in the high concentration groups of the NP exposure. Usually this is related to swelling of the intestine in aging nematodes, in which there is a loss of intestinal nuclei and shortening of microvilli (McGee et al., 2011). If this is the case in nematodes exposed to U, it could support the hypothesis that U affects the assimilation of energy from food as proposed by Goussen et al. (2015). This reduction could in turn explain the delayed development and reproduction observed in the present study. As for the "crookedness" of the intestine at the highest concentration of UO_2 NPs, it is unknown if this is due to loss of structural integrity, or a result of inhibited development.

Other adverse effects included a lower number of oocytes than expected. Unfortunately, images were not taken with this in mind, and often times the oocytes were not completely visibly due to the orientation of the nematode. Thus, preventing a robust statistical analysis. The same went for individuals from the 50 µM UO_2^{2+} ion exposure displaying unusual traits, such as bagging or a deformed pharynx. Future work should focus on getting a more representative set of images in order to determine whether these malignancies were caused by U-toxicity, and if they are specific to one specie.

5.4 Uranium uptake

Uranium uptake was assessed by ICP-MS measurement of exposed N2 nematodes. Measurement of nematodes which had undergone a depuration process after exposure was also performed, in order to differentiate between U on the exterior, and the intestinal lumen of the nematode, and U tightly bound to tissues. The experiment showed that in general, higher U uptake correlated to exposure concentrations. This was with the exception of the 131 µM UO_2 NP exposure where the measured U in the nematodes were lower than expected. The cause for this could be the result of inaccurate pipetting or too few nematodes to determine the U concentration accurately.

Nevertheless the results still show a clear difference between non-depurated and depurated nematodes. It was assumed that the depuration would remove U bound to the exterior of the nematode and the U in the intestinal lumen that had not yet been taken up. Thus, from the results, it seems that a small part (< 10% in most cases) of the U found on each nematode is taken up and retained both in the form of UO_2^{2+} and UO_2 NPs. These results, however, do not show whether measured U concentration was a result of internalized UO_2 NPs, or ions from particle dissolution.

The nematodes exposed to 34.7 μM UO_2 NPs were shown to contain 0.09 pmol U each after depuration. Comparatively, nematodes exposed to 102 μM UO_2^{2+} were also measured to contain 0.09 pmol U after depuration, suggesting that NPs were taken up and retained more easily than ions.

To investigate whether there was a correlation between uptake and effect, uptake was plotted against reproduction and growth in the corresponding concentrations, a regression analysis was performed (Figure 4.4.1 and 4.4.2). These models had higher R^2- values than the models for exposure concentration and effect (Figure 4.3.1), however, this could likely be a result of using fewer data points and not the model having a better fit. This was confirmed by performing a new regression analysis using only the corresponding datapoints from figure 4.3.1 (data not shown), which yielded similarly high R^2-values. Additionally, the measured concentration in the depurated 425 μM UO_2 NP group had a quite high standard deviation. This might be a result of having too few nematodes, or contamination and means that the value can not be trusted. Nevertheless, the regression showed a clear difference between the dose-response of UO_2^{2+} and UO_2 NPs, with the former having a much greater slope number for both reproduction and growth (Figure 4.4.1 and 4.4.2).

From these results it would seem that UO_2 NPs are less toxic than uranyl even if they are more bioavailable. Furthermore, it is unlikely that the UO_2 particles dissolute completely, as this would most likely have resulted in a dose response comparable to that observed in the uranyl exposures. A more likely explanation for the high UO_2 NP concentration observed in the depurated nematodes, is that after ingestion, the nanoparticles were either internalized via endocytosis (Meyer et al., 2010), or were tightly bound to the intestinal gut epithelium. In the environment, particles may under certain conditions dissociate fast and thus release a large amount of uranyl, that may contribute to adverse effects. Similarly, large amounts UO_2^{2+} may be released when contaminated nematodes are ingested by a predator, resulting in bioamplification and adverse effects (Walker et al., 2012).

5.5 Oxidative stress response

Uranium has demonstrated the ability to produce ROS and cause oxidative damage in rodents (Periyakaruppan et al., 2007, Taulan et al., 2004, Taulan et al., 2006). In order to investigate this mechanism of action (MOA) in *C. elegans*, oxidative stress response was assessed using three different reporter strains; SOD-1, HyPer, and GRX. Analysis of the SOD-1 strain revealed a slight but not significant upregulation of *sod-1* in 102 µM UO_2^{2+}, and a significant upregulation in the 460 µM UO_2 NP exposure group.

The microscopy analysis of the HyPer and GRX strains appeared successful with image appearances as expected (See appendix). However, the postprocessing image analysis showed no effect in any treatment (See appendix), which called for reassessment of the raw data fluorescence output signals. This revealed a very high signal intensity, which indicated overexposure of the samples. Unfortunately, this was discovered too late for these analyses to be repeated within the timeframe of this project.

It is tempting to speculate that uranium might have other mechanisms of action. This could for example be formation of complexes with free sulfhydryl groups in proteins, which disrupt metabolic pathways similarly to other heavy metals (Quig, 1998), or imitation of essential ions, such as Ca^{2+} (Arsenault and Hunziker, 1988). Whether the MOA of UO_2^{2+} and UO_2 NP is ROS production or something different, is a topic that should be investigated further in future studies.

5.6 Challenges and future work

After a 96h exposure, the N2 nematodes were stained with Rose Bengal for easier viewing when reproduction, fertility and growth was assessed. Paradoxically, this also lead to the exposure matrix (possibly the *E. coli*) getting stained. This led to the dilemma of either attempting to dilute the content of the well, possibly losing offspring in the process, or working with the low visibility. To get the best possible results, first the grown nematodes and offspring were counted, then the content of the well was diluted before the adult nematodes were measured and checked for eggs. To avoid this in the future, less staining solution should be applied.

When doing fluorescence microscopy of the GM strains of *C. elegans* it was challenging to achieve signals sufficiently high for the software to identify. When using high sensitivity settings on the camera a glare appeared in the image. Eventually this issue was alleviated, somehow, by covering the oculars of the microscope. Still, some of the strains were imaged using sub-optimal settings, which influenced the quality of the images and thus, the results. Ideally, more time should have been spent optimizing the method for imaging.

In this work a limited response in fertility and growth was observed in *C. elegans* from uranyl exposures compared to UO_2 NP exposures. In order to see the full range of effects on reproduction, fertility, growth, and perhaps physiological changes as seen in nematodes exposed to uranium nanoparticles, exposures should be performed using UO_2^{2+} concentrations closer to the 100% mortality dose. Additionally, there was a challenge in maintaining a low pH in the exposure media, possibly reducing the toxicity of the uranyl and UO_2 nanoparticles. Exposing *C. elegans* to higher concentrations of uranyl or in a lower pH, for example 6.7, could likely elicit stronger responses in reproduction, fertility and growth.

It remains unclear whether UO_2 NPs was internalized as particles, or taken up as ions formed by dissolution. One way to investigate this further would be to compare uptake with knock-out strains of *C. elegans* where endocytosis is inhibited. Likewise, metallothioneine knock-out strains could be used to investigate the significance of ions in a UO_2 NP exposures (Jiang et al., 2009, Meyer et al., 2010).

6 Conclusion

The toxicity of UO_2^{2+} and UO_2 NPs in the nematode *C. elegans* was assessed through chronic exposure studies. Both U species was shown to cause a significant decrease in reproduction and growth, while only the NPs caused a measurable decrease in fertility. Overall results indicated a higher toxicity from UO_2^{2+} compared to the UO_2 NPs. Regression analysis revealed a two-fold higher specific dose-response in reproduction from UO_2^{2+} compared to UO_2 NPs. Additionally, effect concentrations for reproduction were calculated for both species. Both EC_{10} and EC_{50} values revealed a higher toxicity from UO_2^{2+} compared to UO_2 NPs. This demonstrates that the UO_2^{2+} ions are more toxic than UO_2 NP in MHRW at pH 7.1-7.4.

The total uptake, as well as retention in depurated nematodes showed a higher uptake of UO_2 NPs than UO_2^{2+}. Thus, the hypothesis that UO_2 NPs are less bioavailable than the UO_2^{2+} was rejected. In the environment, the high uptake may lead to bioamplification if exposed nematodes are ingested by predators.

A significant correlation was found between uptake and effect with both species, showing that effect in reproduction and growth was more sensitive to UO_2^{2+} than UO_2 NP exposure. Thus , UO_2^{2+} is less bioavailable than UO_2 NPs, but had a higher specific toxicity These results corroborate the hypothesis that UO_2^{2+} is the more toxic specie compared to UO_2 NP.

ROS production was investigated as a possible toxic mechanism for UO_2^{2+} and UO_2 NPs. Due to technical challenges however, the analysis of effect of UO_2^{2+} and UO_2 NP on H_2O_2 accumulation and glutathione redox balance, in the HyPer and GRX nematode strains produced no valid results. Nevertheless, the effect on *sod-1* expression suggests that this topic should be investigated further in future studies.

References

ABOSTATE, M. A., SALEH, Y., MIRA, H., AMIN, M., AL KAZINDAR, M. & AHMED, B. M. 2018. Characterization, kinetics and thermodynamics of biosynthesized uranium nanoparticles (UNPs). *Artificial Cells, Nanomedicine, and Biotechnology,* 46**,** 147-159.

AHMED, H., YOUNG, S. D. & SHAW, G. 2014. Factors affecting uranium and thorium fractionation and profile distribution in contrasting arable and woodland soils. *Journal of Geochemical Exploration,* 145**,** 98-105.

ALTUN, Z. F. & HALL, D. H. 2012. *WormAtlas: Handbook of C. elegans Anatomy*.

ARSENAULT, A. L. & HUNZIKER, E. B. 1988. Electron microscopic analysis of mineral deposits in the calcifying epiphyseal growth plate. *Calcified Tissue International,* 42**,** 119-126.

ASIKAINEN, M. & KAHLOS, H. 1979. Anomalously high concentrations of uranium, radium and radon in water from drilled wells in the Helsinki region. *Geochimica et Cosmochimica Acta,* 43**,** 1681-1686.

BACK, P., DE VOS, W. H., DEPUYDT, G. G., MATTHIJSSENS, F., VANFLETEREN, J. R. & BRAECKMAN, B. P. 2012. Exploring real-time in vivo redox biology of developing and aging Caenorhabditis elegans. *Free Radical Biology and Medicine,* 52**,** 850-859.

BANNING, A., DEMMEL, T., RÜDE, T. R. & WROBEL, M. 2013. Groundwater Uranium Origin and Fate Control in a River Valley Aquifer. *Environmental Science & Technology,* 47**,** 13941-13948.

BARBER, D., HANCOCK, S., MCNALLY, A., HINCKLEY, J., BINDER, E., ZIMMERMAN, K., EHRICH, M. & JORTNER, B. 2007. Neurological effects of acute uranium exposure with and without stress. *NeuroToxicology,* 28**,** 1110-1119.

BELOUSOV, V. V., FRADKOV, A. F., LUKYANOV, K. A., STAROVEROV, D. B., SHAKHBAZOV, K. S., TERSKIKH, A. V. & LUKYANOV, S. 2006. Genetically encoded fluorescent indicator for intracellular hydrogen peroxide. *Nature methods,* 3**,** 281-286.

BETTERIDGE, D. J. 2000. What is oxidative stress? *Metabolism,* 49**,** 3-8.

BIGALKE, M., SCHWAB, L., REHMUS, A., TONDO, P. & FLISCH, M. 2018. Uranium in agricultural soils and drinking water wells on the Swiss Plateau. *Environmental Pollution,* 233**,** 943-951.

BIRD, G. A. 2012. Uranium in the Environment: Behavior and Toxicity. *In:* MEYERS, R. A. (ed.) *Encyclopedia of Sustainability Science and Technology.* New York, NY: Springer New York.

BRENNER, S. 1974. The genetics of Caenorhabditis elegans. *Genetics,* 77**,** 71-94.

BRINER, W. & MURRAY, J. 2005. Effects of short-term and long-term depleted uranium exposure on open-field behavior and brain lipid oxidation in rats. *Neurotoxicology and Teratology,* 27**,** 135-144.

BROWN, D. M. 2000. Increased inflammation and intracellular calcium caused by ultrafine carbon black is independent of transition metals or other soluble components. *Occupational and Environmental Medicine,* 57**,** 685-691.

CHARLES, S., VEBER, P. & DELIGNETTE-MULLER, M. L. 2018. MOSAIC: a web-interface for statistical analyses in ecotoxicology. *Environmental Science and Pollution Research,* 25**,** 11295-11302.

CHAZEL, V., HOUPERT, P. & ANSOBORLO, E. 1998. Effect of U3O8 Specific Surface Area on In Vitro Dissolution, Biokinetics, and Dose Coefficients. *Radiation Protection Dosimetry,* 79**,** 39-42.

CHAZEL, V., HOUPERT, P., ANSORBOLO, E., HENGE-NAPOLI, M. H. & PAQUET, F. 2000. Variation of Solubility, Biokinetics and Dose Coefficient of Industrial Uranium Oxides According to the Specific Surface Area. *Radiation Protection Dosimetry,* 88**,** 223-231.

CHOPPIN, G., LILJENZIN, J.-O., RYDBERG, J. & EKBERG, C. 2014. *Radiochemistry and nuclear chemistry,* Amsterdam, Elsevier.

CHOPPIN, G. R. 2007. Actinide speciation in the environment. *Journal of Radioanalytical and Nuclear Chemistry,* 273**,** 695-703.

COYLE, P., PHILCOX, J. C., CAREY, L. C. & ROFE, A. M. 2002. Metallothionein: the multipurpose protein. *Cellular and Molecular Life Sciences (CMLS),* 59**,** 627-647.

ČUBA, V., PROCHÁZKOVÁ, L., BÁRTA, J., VONDRÁŠKOVÁ, A., PAVELKOVÁ, T., MIHÓKOVÁ, E., JARÝ, V. & NIKL, M. 2014. UV radiation: a promising tool in the synthesis of multicomponent nano-oxides. 16.

DANESI, P. R., MARKOWICZ, A., CHINEA-CANO, E., BURKART, W., SALBU, B., DONOHUE, D., RUEDENAUER, F., HEDBERG, M., VOGT, S., ZAHRADNIK, P. & CIURAPINSKI, A. 2003. Depleted uranium particles in selected Kosovo samples. *Journal of Environmental Radioactivity,* 64**,** 143-154.

DE MATTEIS, V. & RINALDI, R. 2018. Toxicity Assessment in the Nanoparticle Era. Springer International Publishing.

DICKSON, J. S. & KOOHMARAIE, M. 1989. Cell surface charge characteristics and their relationship to bacterial attachment to meat surfaces. *Applied and Environmental Microbiology,* 55**,** 832-836.

DONALDSON, K. 2004. Nanotoxicology. *Occupational and Environmental Medicine,* 61**,** 727-728.

DOONAN, R., MCELWEE, J. J., MATTHIJSSENS, F., WALKER, G. A., HOUTHOOFD, K., BACK, P., MATSCHESKI, A., VANFLETEREN, J. R. & GEMS, D. 2008. Against the oxidative damage theory of aging: superoxide dismutases protect against oxidative stress but have little or no effect on life span in Caenorhabditis elegans. *Genes & Development,* 22**,** 3236-3241.

DUTILLEUL, M., LEMAIRE, L., RÉALE, D., LECOMTE, C., GALAS, S. & BONZOM, J.-M. 2013. Rapid phenotypic changes in Caenorhabditis elegans under uranium exposure. *Ecotoxicology,* 22**,** 862-868.

ELLEGAARD-JENSEN, L., JENSEN, K. A. & JOHANSEN, A. 2012. Nano-silver induces dose-response effects on the nematode Caenorhabditis elegans. *Ecotoxicology and Environmental Safety,* 80**,** 216-223.

ELLIOT, W. H. & ELLIOT, D. C. 2009. *Biochemistry and Molecular Biology,* Oxford, New York, Oxford University Press.

FORTIN, C., DUTEL, L. & GARNIER-LAPLACE, J. 2004. URANIUM COMPLEXATION AND UPTAKE BY A GREEN ALGA IN RELATION TO CHEMICAL SPECIATION: THE IMPORTANCE OF THE FREE URANYL ION. *Environmental Toxicology and Chemistry,* 23**,** 974.

FRENGSTAD, B., MIDTGÅRD SKREDE, A. K., BANKS, D., REIDAR KROG, J. & SIEWERS, U. 2000. The chemistry of Norwegian groundwaters: III. The distribution of trace elements in 476 crystalline bedrock groundwaters, as analysed by ICP-MS techniques. *Science of The Total Environment,* 246**,** 21-40.

GHAFOURI, S. & MCGHEE, J. 2007. Bacterial residence time in the intestine of Caenorhabditis elegans. *Nematology,* 9**,** 87-91.

GOUSSEN, B., BEAUDOUIN, R., DUTILLEUL, M., BUISSET-GOUSSEN, A., BONZOM, J.-M. & PÉRY, A. R. R. 2015. Energy-based modelling to assess effects of chemicals on Caenorhabditis elegans: A case study on uranium. *Chemosphere,* 120**,** 507-514.

GOUSSEN, B., PARISOT, F., BEAUDOUIN, R., DUTILLEUL, M., BUISSET-GOUSSEN, A., PÉRY, A. R. R. & BONZOM, J.-M. 2013. Consequences of a multi-generation exposure to uranium on Caenorhabditis elegans life parameters and sensitivity. *Ecotoxicology,* 22**,** 869-878.

GUÉGUEN, Y., ROY, L., HORNHARDT, S., BADIE, C., HALL, J., BAATOUT, S., PERNOT, E., TOMASEK, L., LAURENT, O., EBRAHIMIAN, T., IBANEZ, C., GRISON, S., KABACIK, S., LAURIER, D. & GOMOLKA, M. 2017. Biomarkers for Uranium Risk Assessment for the Development of the CURE (Concerted Uranium Research in Europe) Molecular Epidemiological Protocol. *Radiation Research,* 187**,** 107-127.

GUTSCHER, M., PAULEAU, A.-L., MARTY, L., BRACH, T., WABNITZ, G., SAMSTAG, Y., MEYER, A. & DICK, T. 2008. Real-time imaging of the intracellular glutathione redox potential. *Nature methods,* 5**,** 553-9.

HAMILTON, M. M., EJNIK, J. W. & CARMICHAEL, A. J. 1997. Uranium reactions with hydrogen peroxide studied by EPR–spin trapping with DMPO †. *Journal of the Chemical Society, Perkin Transactions 2***,** 2491-2494.

HANDY, R. D., VAN DEN BRINK, N., CHAPPELL, M., MÜHLING, M., BEHRA, R., DUŠINSKÁ, M., SIMPSON, P., AHTIAINEN, J., JHA, A. N., SEITER, J., BEDNAR, A., KENNEDY, A., FERNANDES, T. F. & RIEDIKER, M. 2012. Practical considerations for conducting ecotoxicity test methods with manufactured nanomaterials: what have we learnt so far? *Ecotoxicology,* 21**,** 933-972.

HUDRY, D., GRIVEAU, J.-C., APOSTOLIDIS, C., WALTER, O., COLINEAU, E., RASMUSSEN, G., WANG, D., CHAKRAVADHALUNA, V. S. K., COURTOIS, E., KÜBEL, C. & MEYER, D. 2014. Thorium/uranium mixed oxide nanocrystals: Synthesis, structural characterization and magnetic properties. *Nano Research,* 7**,** 119-131.

HURAULT, L., CREFF, G., HAGÈGE, A., SANTUCCI-DARMANIN, S., PAGNOTTA, S., FARLAY, D., DEN AUWER, C., PIERREFITE-CARLE, V. & CARLE, G. F. 2019. Uranium Effect on Osteocytic Cells In Vitro. *Toxicological Sciences,* 170**,** 199-209.

HYNE, R. V., RIPPON, G. D. & ELLENDER, G. 1992. pH-Dependent uranium toxicity to freshwater hydra. *STOTEN</cja:jid> Science of the Total Environment,* 125**,** 159-173.

ISO/TC 147/SC 5 2010. *ISO 10872:2010 Water quality - determination of the toxic effect of sediment and soil samples on the growth, fertiility and reproduction of Caenorhabditis elegans (Nematoda)*

JIANG, G. C. T., HUGHES, S., STÜRZENBAUM, S. R., EVJE, L., SYVERSEN, T. & ASCHNER, M. 2009. Caenorhabditis elegans Metallothioneins Protect against Toxicity Induced by Depleted Uranium. *Toxicological Sciences,* 111**,** 345-354.

KIYAMA, Y., MIYAHARA, K. & OHSHIMA, Y. 2012. Active uptake of artificial particles in the nematode Caenorhabditis elegans. *Journal of Experimental Biology,* 215**,** 1178-1183.

KNAAPEN, A. M., BORM, P. J. A., ALBRECHT, C. & SCHINS, R. P. F. 2004. Inhaled particles and lung cancer. Part A: Mechanisms. *International Journal of Cancer,* 109**,** 799-809.

KULKARNI, S., MISRA, C. S., GUPTA, A., BALLAL, A. & APTE, S. K. 2016. Interaction of Uranium with Bacterial Cell Surfaces: Inferences from Phosphatase-Mediated Uranium Precipitation. *Applied and Environmental Microbiology,* 82**,** 4965-4974.

KUMAR, A. & DIXIT, C. 2017. 3. Methods for characterization of nanoparticles.

LEMERCIER, V., MILLOT, X., ANSOBORLO, E., F, A, ROUSSELLE, C. & M. SCHERRMANN, J. 2003. Study of uranium transfer across the blood-brain barrier. *Radiation Protection Dosimetry,* 105**,** 243-245.

LINDBERG, H. K., FALCK, G. C. M., CATALÁN, J., KOIVISTO, A. J., SUHONEN, S., JÄRVENTAUS, H., ROSSI, E. M., NYKÄSENOJA, H., PELTONEN, Y., MORENO, C., ALENIUS, H., TUOMI, T., SAVOLAINEN, K. M. & NORPPA, H. 2012. Genotoxicity of inhaled nanosized TiO2 in mice. *Mutation Research/Genetic Toxicology and Environmental Mutagenesis,* 745**,** 58-64.

LIU, F., DU, K.-J., FANG, Z., YOU, Y., WEN, G.-B. & LIN, Y.-W. 2015. Chemical and biological insights into uranium-induced apoptosis of rat hepatic cell line. *Radiation and Environmental Biophysics,* 54**,** 207-216.

LU, M., LI, H., LI, Y., LU, Y., WANG, H. & WANG, X. 2020. Exploring the Toxicology of Depleted Uranium with Caenorhabditis elegans. *ACS Omega,* 5**,** 12119-12125.

MA, H., BERTSCH, P. M., GLENN, T. C., KABENGI, N. J. & WILLIAMS, P. L. 2009. TOXICITY OF MANUFACTURED ZINC OXIDE NANOPARTICLES IN THE NEMATODE CAENORHABDITIS ELEGANS. *Environmental Toxicology and Chemistry,* 28**,** 1324.

MALVERN INSTRUMENTS 2013. *Zetasizer Nano user manual*

MANGO, S. 2007. The C. elegans pharynx: a model for organogenesis. *WormBook*.

MASARUDIN, M. J., CUTTS, S. M., EVISON, B. J., PHILLIPS, D. R. & PIGRAM, P. J. 2015. Factors determining the stability, size distribution, and cellular accumulation of small, monodisperse chitosan nanoparticles as candidate vectors for anticancer drug delivery: application to the passive encapsulation of [14C]-doxorubicin. *Nanotechnology, Science and Applications***,** 67.

MASSARIN, S., BEAUDOUIN, R., ZEMAN, F., FLORIANI, M., GILBIN, R., ALONZO, F. & PERY, A. R. 2011. Biology-based modeling to analyze uranium toxicity data on Daphnia magna in a multigeneration study. *Environ Sci Technol,* 45**,** 4151-8.

MCGEE, M. D., WEBER, D., DAY, N., VITELLI, C., CRIPPEN, D., HERNDON, L. A., HALL, D. H. & MELOV, S. 2011. Loss of intestinal nuclei and intestinal integrity in aging C. elegans. *Aging Cell,* 10**,** 699-710.

MEYER, J. N., LORD, C. A., YANG, X. Y., TURNER, E. A., BADIREDDY, A. R., MARINAKOS, S. M., CHILKOTI, A., WIESNER, M. R. & AUFFAN, M. 2010. Intracellular uptake and associated toxicity of silver nanoparticles in Caenorhabditis elegans. *Aquatic Toxicology,* 100**,** 140-150.

MILLER, A. C., XU, J., STEWART, M., BROOKS, K., HODGE, S., SHI, L., PAGE, M. & MCCLAIN, D. 2002. Observation of Radiation-specific Damage in Human Cells Exposed to Depleted Uranium: Dicentric Frequency and Neoplastic Transformation as Endpoints. *Radiation Protection Dosimetry,* 99**,** 275-278.

MURPHY, D. B. & DAVIDSON, M. W. 2013. *Fundamentals of light microscopy and electronic imaging,* Hoboken, N.J., Wiley-Blackwell.

MÖRCK, C., AXÄNG, C. & PILON, M. 2003. A genetic analysis of axon guidance in the C. elegans pharynx. *Developmental Biology,* 260**,** 158-175.

NOWACK, B. & BUCHELI, T. D. 2007. Occurrence, behavior and effects of nanoparticles in the environment. *Environmental Pollution,* 150**,** 5-22.

OEDA, T. 2001. Oxidative stress causes abnormal accumulation of familial amyotrophic lateral sclerosis-related mutant SOD1 in transgenic Caenorhabditis elegans. 10**,** 2013-2023.

PAVELKOVÁ, T., ČUBA, V., DE VISSER-TÝNOVÁ, E., EKBERG, C. & PERSSON, I. 2016. Preparation of UO2, ThO2 and (Th,U)O2 pellets from photochemically-prepared nano-powders. 469**,** 57-61.

PAVELKOVÁ, T., ČUBA, V. & SEBESTA, F. 2013. Photo-induced low temperature synthesis of nanocrystalline UO2, ThO2 and mixed UO2-ThO2 oxides. *Journal of Nuclear Materials,* 442**,** 29-32.

PELLMAR, T. 1999. Distribution of uranium in rats implanted with depleted uranium pellets. *Toxicological Sciences,* 49**,** 29-39.

PERIYAKARUPPAN, A., KUMAR, F., SARKAR, S., SHARMA, C. S. & RAMESH, G. T. 2007. Uranium induces oxidative stress in lung epithelial cells. *Archives of Toxicology,* 81**,** 389-395.

PETITOT, F., LESTAEVEL, P., TOURLONIAS, E., MAZZUCCO, C., JACQUINOT, S., DHIEUX, B., DELISSEN, O., TOURNIER, B. B., GENSDARMES, F., BEAUNIER, P. & DUBLINEAU, I. 2013. Inhalation of uranium nanoparticles: Respiratory tract deposition and translocation to secondary target organs in rats. *Toxicology Letters,* 217**,** 217-225.

PFEIFFER, C., REHBOCK, C., HÜHN, D., CARRILLO-CARRION, C., DE ABERASTURI, D. J., MERK, V., BARCIKOWSKI, S. & PARAK, W. J. 2014. Interaction of colloidal nanoparticles with their local environment: the (ionic) nanoenvironment around nanoparticles is different from bulk and determines the physico-chemical properties of the nanoparticles. *Journal of The Royal Society Interface,* 11**,** 20130931.

PLATEL, A., CARPENTIER, R., BECART, E., MORDACQ, G., BETBEDER, D. & NESSLANY, F. 2016. Influence of the surface charge of PLGA nanoparticles on theirin vitrogenotoxicity, cytotoxicity, ROS production and endocytosis. *Journal of Applied Toxicology,* 36**,** 434-444.

QUIG, D. 1998. Cysteine Metabolism and Metal Toxicity. *Alternative medicine review : a journal of clinical therapeutic,* 3**,** 262-70.

REJMAN, J., OBERLE, V., ZUHORN, I. S. & HOEKSTRA, D. 2004. Size-dependent internalization of particles via the pathways of clathrin- and caveolae-mediated endocytosis. *Biochemical Journal,* 377**,** 159-169.

RIDDLE, D. L., BLUMENTHAL, T., MEYER, B. J. & PRIESS, J. R. 1997. *C. elegans II,* Plainview, N.Y, Cold Spring Harbor Laboratory Press.

RISOM, L., MØLLER, P. & LOFT, S. 2005. Oxidative stress-induced DNA damage by particulate air pollution. *Mutation Research/Fundamental and Molecular Mechanisms of Mutagenesis,* 592**,** 119-137.

ROSSBACH, L. M. 2019. Single and multigenerational studies of silver nanoparticle toxicity and adaptive mechanisms in the nematode Caenorhabditis elegans.

RSC 2001. The Health Hazards of Depleted Uranium Munitions, Part 1. Policy Document 6/01. *The Royal Society of Chemistry*, 1-80.

SALBU, B., JANSSENS, K., LIND, O. C., PROOST, K., GIJSELS, L. & DANESI, P. R. 2005. Oxidation states of uranium in depleted uranium particles from Kuwait. *Journal of Environmental Radioactivity,* 78, 125-135.

SANDERSON, M. J., SMITH, I., PARKER, I. & BOOTMAN, M. D. 2014. Fluorescence Microscopy. *Cold Spring Harbor Protocols,* 2014, pdb.top071795-p.

SHEN, L., XIAO, J., YE, H. & WANG, D. 2009. Toxicity evaluation in nematode Caenorhabditis elegans after chronic metal exposure. *Environmental Toxicology and Pharmacology,* 28, 125-132.

SKOOG, D. A., HOLLER, F. J. & CROUCH, S. R. 2018. *Principles of instrumental analysis*.

STETEFELD, J., MCKENNA, S. A. & PATEL, T. R. 2016. Dynamic light scattering: a practical guide and applications in biomedical sciences. *Biophysical reviews,* 8, 409-427.

STIERNAGLE, T. 2006. Maintenance of C. elegans, WormBook.

SWAIN, S. C., KEUSEKOTTEN, K., BAUMEISTER, R. & STÜRZENBAUM, S. R. 2004. C. elegans metallothioneins: new insights into the phenotypic effects of cadmium toxicosis. *J Mol Biol,* 341, 951-59.

TAULAN, M., PAQUET, F., ARGILES, A., DEMAILLE, J. & ROMEY, M.-C. 2006. Comprehensive analysis of the renal transcriptional response to acute uranyl nitrate exposure. *BMC Genomics,* 7.

TAULAN, M., PAQUET, F., MAUBERT, C., DELISSEN, O., DEMAILLE, J. & ROMEY, M.-C. 2004. Renal Toxicogenomic Response to Chronic Uranyl Nitrate Insult in Mice. *Environmental Health Perspectives,* 112, 1628-1635.

THE C. ELEGANS SEQUENCING CONSORTIUM 1998. Genome Sequence of the Nematode C. elegans: A Platform for Investigating Biology. *Science,* 282, 2012-2018.

TYNE, W., LOFTS, S., SPURGEON, D. J., JURKSCHAT, K. & SVENDSEN, C. 2013. A new medium for Caenorhabditis elegans toxicology and nanotoxicology studies designed to better reflect natural soil solution conditions. *Environmental Toxicology and Chemistry,* 32, 1711-1717.

UIJT DE HAAG, P. A. M., SMETSERS, R. C. G. M., WITLOX, H. W. M., KRÜS, H. W. & EISENGA, A. H. M. 2000. Evaluating the risk from depleted uranium after the Boeing 747-258F crash in Amsterdam, 1992. *Journal of Hazardous Materials,* 76, 39-58.

VANLOON, G. W. & DUFFY, S. J. 2011. *Environmental chemistry : a global perspective,* Oxford; Toronto, Oxford University Press.

WALKER, C. H., SIBLY, R. M., HOPKIN, S. P. & PEAKALL, D. B. 2012. *Principles of ecotoxicology,* Boca Raton, FL, CRC Press.

WILLIAMS, D. B. & CARTER, C. B. 2009. *Transmission Electron Microscopy: A Textbook for Materials Science*, Springer.

WILTSCHE, H., WINKLER, M. & TIRK, P. 2015. Matrix effects of carbon and bromine in inductively coupled plasma optical emission spectrometry. *Journal of Analytical Atomic Spectrometry,* 30, 2223-2234.

WU, Y., WANG, Y. & GUO, W. 2019. Behavior and fate of geogenic uranium in a shallow groundwater system. *Journal of Contaminant Hydrology,* 222, 41-55.

ZAMORA, M. 1998. Chronic Ingestion of Uranium in Drinking Water: A Study of Kidney Bioeffects in Humans. 43, 68-77.

ZEMAN, F. A., GILBIN, R., ALONZO, F., LECOMTE-PRADINES, C., GARNIER-LAPLACE, J. & ALIAUME, C. 2008. Effects of waterborne uranium on survival, growth, reproduction and physiological processes of the freshwater cladoceran Daphnia magna. *Aquatic Toxicology,* 86, 370-378.

ZHANG, X., SERVOS, M. R. & LIU, J. 2012. Ultrahigh Nanoparticle Stability against Salt, pH, and Solvent with Retained Surface Accessibility via Depletion Stabilization. *Journal of the American Chemical Society,* 134, 9910-9913.

Appendix – Results from HyPer and GRX analysis

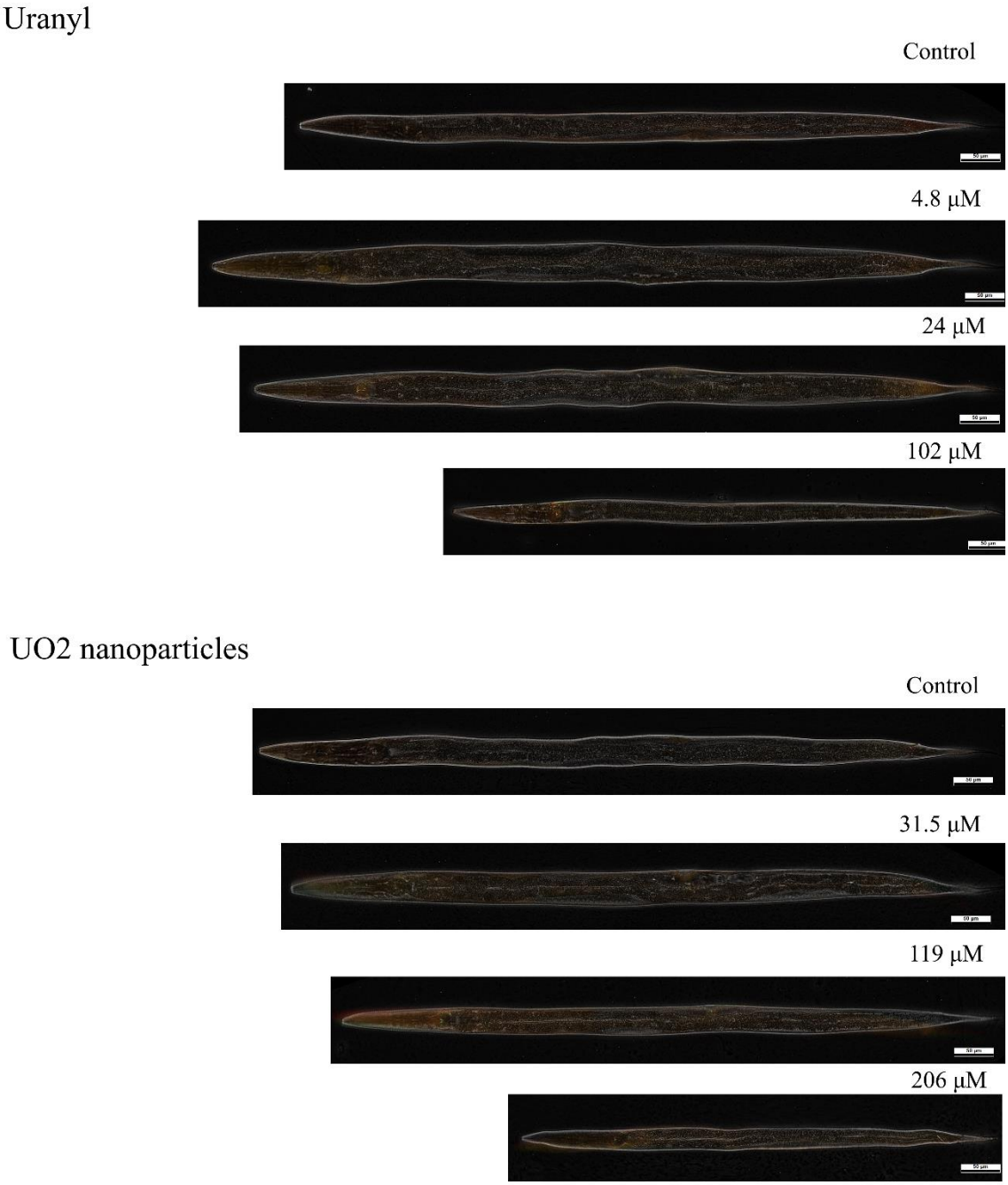

Figure i: Representative examples of phase contrast images taken of HyPer strain nematodes exposed to uranyl and UO_2 nanoparticles at 72h. Images are overlayed with both reduced (red) and oxidized (green) fluorescence channels. Nematodes were straightened using ImageJ and 50 µm scalebars are included in each micrograph.

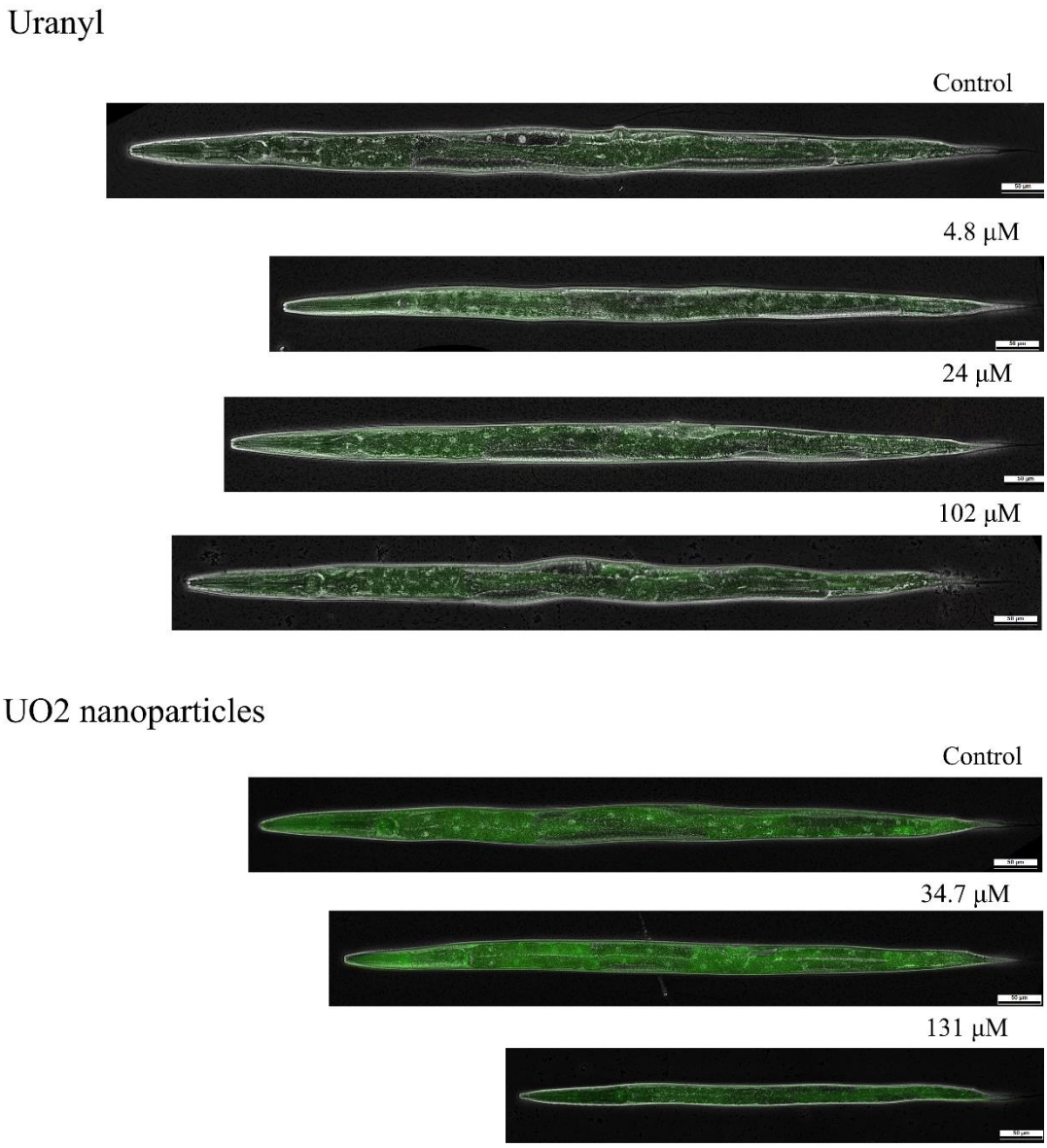

Figure ii: Representative examples of phase contrast images with taken of GRX strain nematodes exposed to uranyl and UO_2 nanoparticles at 72h. Images are overlayed with both reduced (green) and oxidized (red) fluorescence channels. Nematodes were straightened using ImageJ and 50 µm scalebars are included in each micrograph.

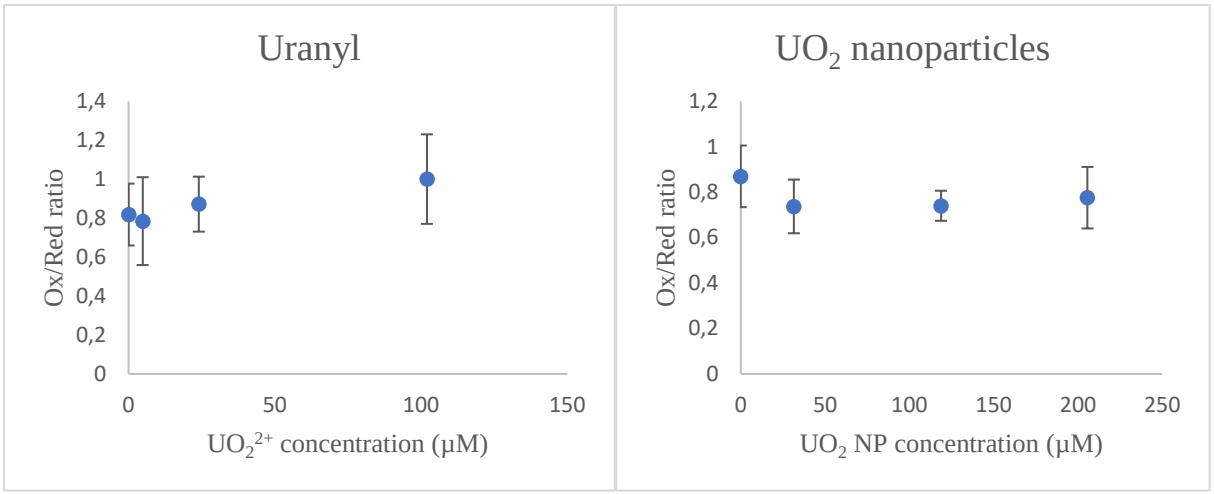

Figure: iii: Ratio between "oxidized" and "reduced" signal in HyPer nematodes exposed to different concentrations of U in the form of ions and nanoparticles.

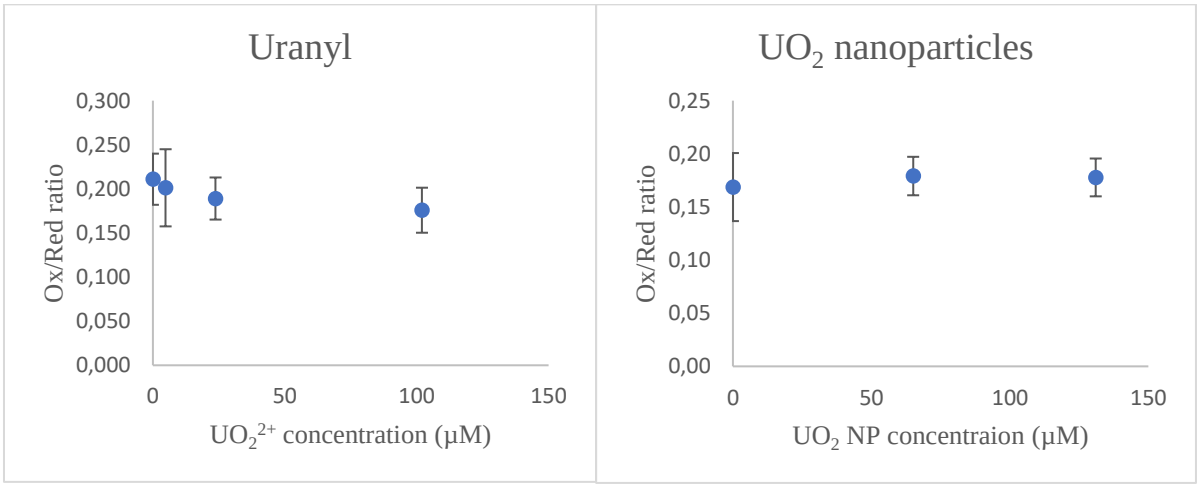

Figure iv: Ratio between "oxidized" and "reduced" signal in GRX nematodes exposed to different concentrations of U in the form of ions and nanoparticles.

Norges miljø- og biovitenskapelige universitet
Noregs miljø- og biovitskapelege universitet
Norwegian University of Life Sciences

Postboks 5003
NO-1432 Ås
Norway